Super-Convincing asd Thesis Title

A Thesis Presented

by

Aly Sultan

to

The Department of Electrical and Computer Engineering

in partial fulfillment of the requirements

for the degree of

Master of Science

in

Electrical and Computer Engineering

Northeastern University
Boston, Massachusetts

MM YYYY

NORTHEASTERN UNIVERSITY

Graduate School of Engineering

Thesis Title: Super-Convincing asd Thesis Title

Author: Aly Sultan.

Department: Electrical and Computer Engineering.

Approved for Thesis Requirements of the Master of Science Degree

Thesis Advisor: Professor Gunar Schirner	Date
Thesis Reader: AA BB	Date
Thesis Reader: CC DD	Date
Department Chair: ZZ EE	Date

Director of the Graduate School:

Dean: EE FF	Date

To my family.

Contents

List of Figures

List of Tables

List of Acronyms

ASIC Application Specific Integrated Circuit.

FPGA Field Programmable Gate Array.

GEMM General Matrix Multiplication.

CNN ConvoluTional Neural Network.

DNN Deep Neural Network.

ACC Accelerator.

Conv Convolution.

MAC Multiply and Accumulate.

PE Processing Engine.

HERO-T Hybrid GEMM and Direct Convolution Accelerator Template

FC Fully Connected

SAM Self Addresable Memory

HERO-T-Sim HERO-T simulator

TEMPO accelerator TEMPlate Optimizer.

CIGAR ConvoluTional neural network Statistics GAtheRer.

SAM Self Addressable SRAMs.

Acknowledgments

Here I wish to thank those who have supported me during the process of the thesis work....

Abstract of the Thesis

Super-Convincing asd Thesis Title

by

Aly Sultan

Master of Science in Electrical and Computer Engineering

Northeastern University, MM YYYY

Professor Gunar Schirner, Adviser

This is a very abstract abstract.

Chapter 1

Introduction

1.1 AI and Edge Computing

Deep Neural Network (DNN)s currently represent the state of the art in complex regression and classification problems in image recognition, sequence to sequnce learning [12], speech recognition [2]. As such they are being deployed on both cloud platforms and edge devices at scale.

ConvoluTional Neural Network (CNN)s are a variant of DNNs that demonstrate great accuracy in image/video recognition. The main computation layer of CNNs that consumes most of the runtime of a network is the convolutional layer. A convolution layer operates on multi-demension tensors as part of a CNNs feature extraction portion of the network. (Citation needed). Convolution layers exhibit a significant amount of parallel behavior and data reuse. Additionally, the tight latency, throughout and energy constraints imposed on CNN's in various enviornments, particularly on edge devices has led to the proliferation of customized hardware accelerators for CNNs with particular emphasis on accelerating convolution layers.

1.2 Convolution accelerators

Citation Needed Prior work on CNN accelerators design can broadly be classified based on 1) their target execution platform Application Specific Integrated Circuit (ASIC)/Field Programmable Gate Array (FPGA) 2) Their target for acceleration, either entire layers of the network or specifically convolution layers and finally 3) Their mathematical interpretation of the convolution operation as either fundementally a matrix operation post reorganization of its input tensor or

1

a conventional stencil based operation. In the next section, the strengths and weaknesses of the afformentioned approaches will be discussed.

1.3 Problem Definition

Regardless of the target execution platform chosen for a novel CNN accelerator architecture there exists a need to create a general enough architecture that can support a wide variety of networks and network layer types. CNN Accelerator (ACC) generality can be decomposed into 1) Convolution generality, which can be defined as the range of support convolution layers and 2) Network generality, whcih can be defined as the types convolution network layers supported

FPGAs inherently have an advantage w.r.t architecture generality given their reconfigurable nature. FPGA-centric approaches incorporate the architecture of a target CNN network into their architecture compilation process [16]. This allows FPGA-based architectures to tackle network generality by adding layer-spcific accelerators (provided they are available) at compile time, as well as tailor Convolution (Conv) ACC primitives to the target network in order to provide the appropriate amount of Conv generality and performance. The disadvantage of FPGA based architectures is 1) The need to recompile the architecture prior to deployment of a new CNN with possibly no support for a new CNN without recompilation 2) Inferior performance and energy efficiency compared to a hardened architecture. One could harden a design produced by an FPGA-based architecture compilation process. However, this will produce a design optimized for only one network and may not be general enough. To the best of this author's knoweldge, no FPGA-based ACC compilation processes incorporate more than one CNN network architectures into their architecture optimization process.

ASIC-based architectures tackle network generality by introducing a wide variety of hardened layer accelerator primitives on-chip (CITE TPU). Additionally, they tackle convolution generality by either 1) Reinterpreting convolution layers as GEMM operations (CITE TPU and GEMMINI) or 2) Creating a general enough Conv ACC capable of supporting a wide range of Conv layer dimensions directly (CITE EYERISS). Given the pace of development in DNNs, new layers like (CITE ATTENTION IS ALL YOU NEED)'s self attention layer can arise and become integral to improving DNN model performance [3]. These new layers may not be fully compatabile with the chosen accelerator primitives in the ASIC-based design approach and as a result may only be partially accelerated. Additionally, ASIC-based designs must balance their dediction of on-chip resources to convolution vs other resource intensive layers (e.g Fully Connected (FC) layers) which

may cause convolution performance to suffer. Approaches that reinterpret convolutions to increase convolution generality like GEMM tend to dramatically increase data volume which may strain on-chip memory resources as well as decrease energy efficicency [16]. Finally, supporting a wide range of convolutions can come at the cost of reduced performance/ energy efficiency for the statistical common case of convolutions layer dimensions in a wide range of CNNs.

1.4   Solution Overview

There exists a convolution accelerator architectural template that offers 1) Improved performance/ energy efficiency for the common case of convolution layers accross a broad range of CNNs 2) Operational flexibility to be able to compute a wide variety of convolution layers under various and possibly uncommon configurations 3) The ability to partially or fully accelerate computationally intensive layers that currently exist in the literature and ones that may arise in the future 4) The configurability that enables the architectural template to be modified based on available compute resources and a target library of networks. To satisfy the afformentioned requirements, in this thesis, the following is proposed:

1. A Hybrid GEMM and Direct Convolution Accelerator Template (HERO-T)

2. Self Addressable SRAMs (SAM) a novel on-chip memory primitive capable of orchestrating energy efficient on chip data movements within HERO-T

3. (ConvolutIon statIstics GAthere) CIGAR a tool that enables HERO-T's data driven design of HERO-T

4. accelerator TEMPlate Optimizer (TEMPO) a tool that optimizes HERO-T based on a target CNN library and available compute resources

5. HERO-T simulator (HERO-T-Sim) a cycle SystemC model of HERO-T combined with a python evaluation frontend that assesses a concrete HERO-T instance's performance and energy efficiency on a target CNN library

1.5   Thesis Structure

Chapter 2

Background

To motivate the architecture design space introduce in chapter (REFERENCE chapter) I first need to 3) show how to convert a convolution operation into a GEMM 4) Introduce dataflow exploration through direct representation if implementing an accelerates that accelerates convolutions directly 5) Introduce hardware + based on reuse behavior in the Dataflow dataflow -¿ describes communication -¿ describes datareuse 6) Introduce polyhedral model to evaluate temporal reuse behavior In this chapter I breakdown what convolutions are mathetmatically

Figure 2.1
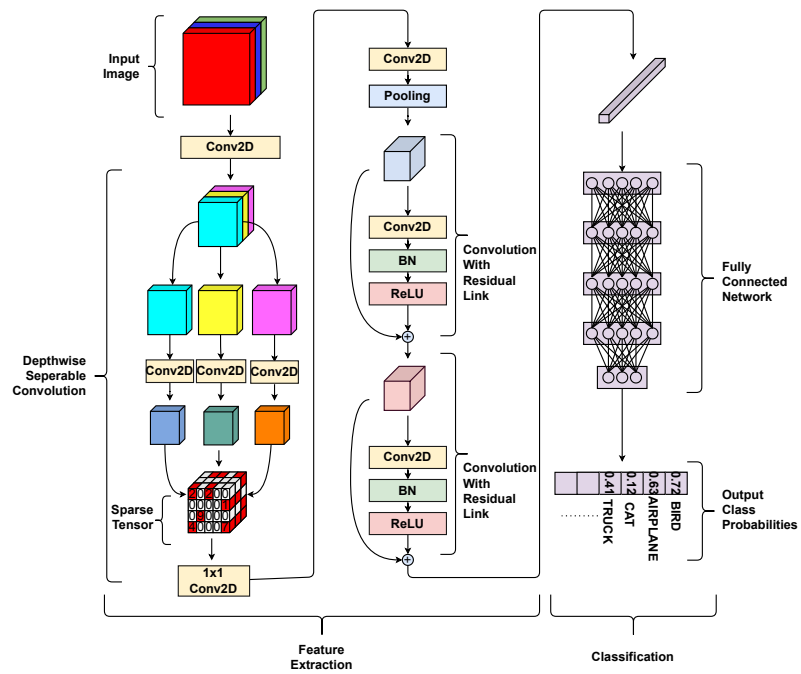
Figure 2.1: Example Image Classfication CNN

2.1 The Math behind convolutions

1) explain what convolutions are mathematically
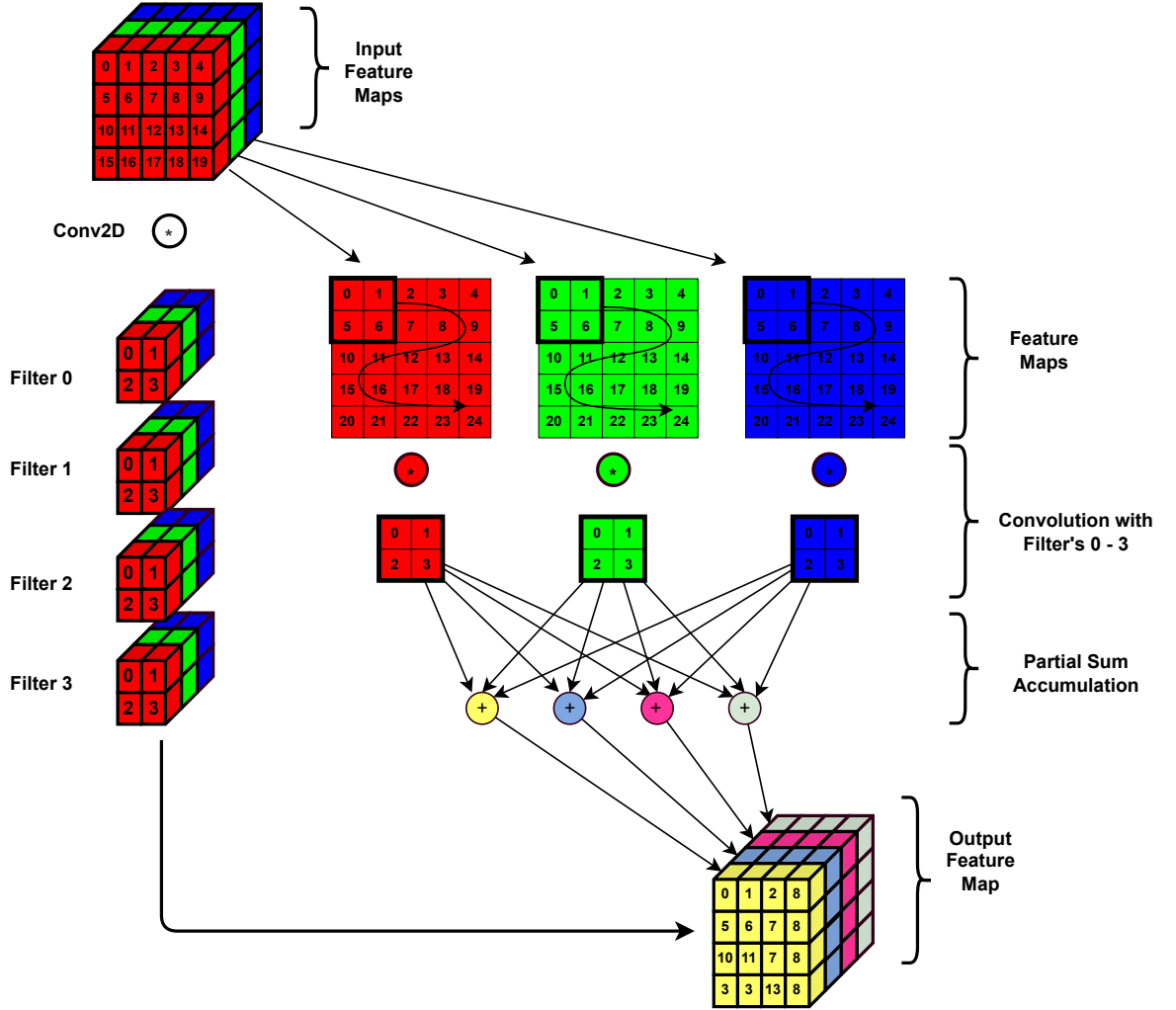
Figure 2.2: Convolution Operation Illustrated

$$IFmap \in R^{C \times n \times n}$$
$$OFmap \in R^{F \times m \times m} \tag{2.1}$$
$$Weight \in R^{F \times C \times K \times K}$$

$$OFmap[f][y][x] = \sum_{c=0}^{C-1} \sum_{k_x=0}^{K-1} \sum_{k_y=0}^{K-1} Weight[f][c][k_y][k_x] * IFmap[c][y+ky][x+kx] \quad (2.2)$$

2.2 Loop Based Representation Of Convolutions

Direct naive implementation of **??** with tensors Equation 2.1 as a series of loops is given below Listing 3.1

Listing 2.1: Convolution implemented as nested loops

```
1   for(int f = 0; f < F; f++) // Filter loop
2       for(int c = 0; c < C; c++) // Channel loop
3           for(int y = 0; y < Y; y++) // Output feature map row
4               for(int x = 0; x < X; x++)  // Output feature map col
5                   for(int ky = 0; ky < KY; ky++)  // Kernel row
6                       for(int kx = 0; kx < KX; kx++)  // Kernel col
7                           O[f][y][x] += I[c][y+ky][x+kx]*W[f][c][ky][kx];
```

2.3 Convolution as general matrix multiplication
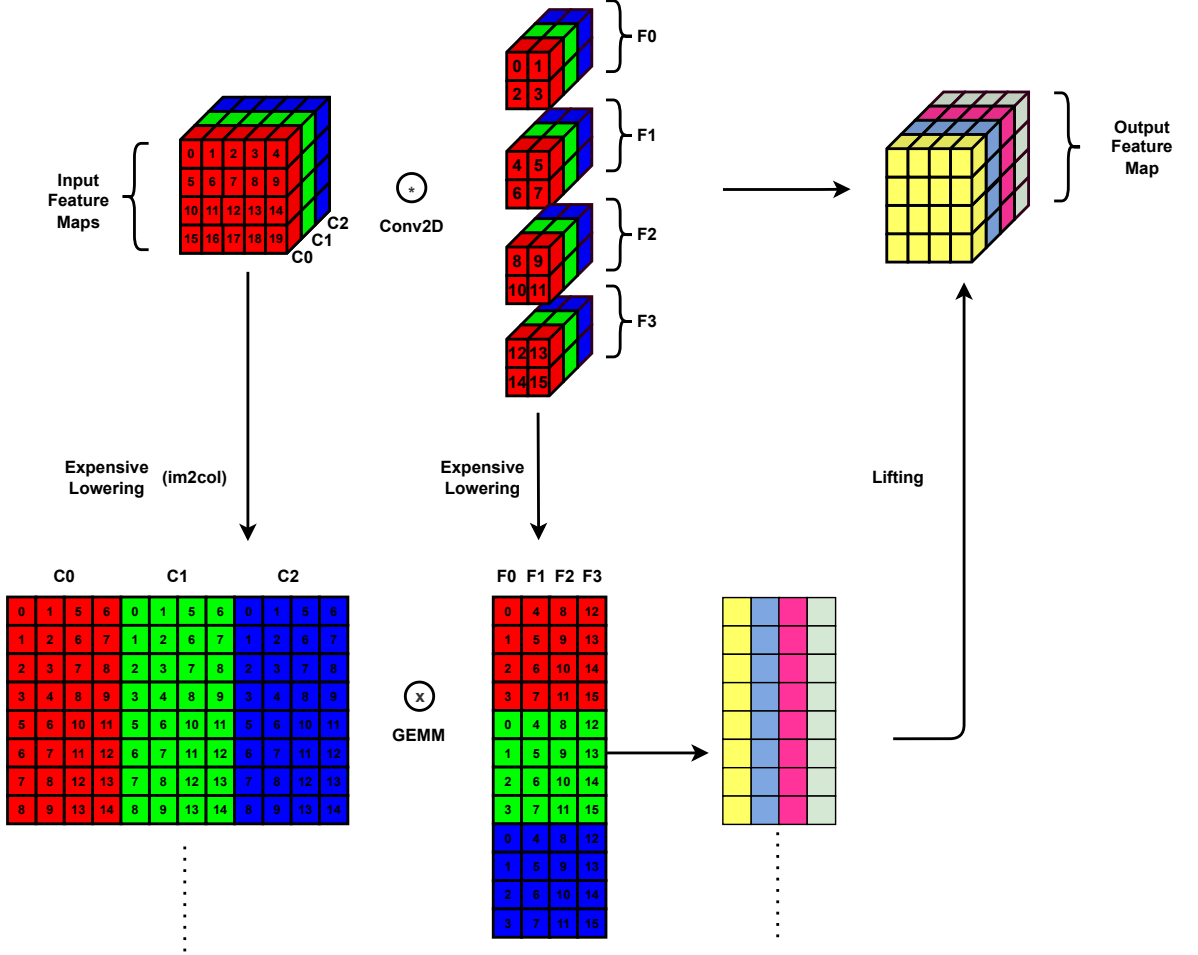
Figure 2.3: Im2Col Illustrated

Convolution can be converted into a GEMM

Popular techniques like im2col (illustrated in Figure 2.3) can be used to convert any convolution operation into GEMM (listed as expensive lowering [1]) but there are others techniques that don't produce such massive input feature maps

If willing to increase complexity of lowering of ifmap and weight tensors after GEMM we can reduce bloat in ifmap with balanced lifting/ loading in [1]. Analytical expressions adapted from [1] are given below with the inclusion of lowering in the presence of multiple filters.

$$IFmap \in R^{C \times n \times n} \xrightarrow{BalancedLowering} \hat{IFmap} \in R^{nm \times KC}$$

$$\hat{IFmap}[cn + r, :] = vec(IFmap[:, r, c : c + K]) \tag{2.3}$$

$$\forall r, c \in [0, n-1], [0, m-1]$$

$$Weight \in R^{F \times C \times K \times K} \xrightarrow{BalancedLowering} \hat{Weight} \in R^{KC \times FK}$$

$$\hat{Weight}[f * K : f * K + K, i] = vec(Weight[f, :, i, :]) \tag{2.4}$$

$$\forall f, i \in [0, F-1], [0, K-1]$$

In balanced lowering, we first lower the ifmap and weights using expression (2.3) and (2.4).

$$\hat{OFmap} = \hat{IFmap}.\hat{Weight} \tag{2.5}$$

Then a GEMM is performed (2.5)

$$\hat{OFmap} \in R^{nm \times FK} \xrightarrow{BalancedLifting} OFmap \in R^{m \times m \times F}$$

$$OFmap[f, r, c] = \left(\sum_{j=0}^{K-1} \hat{OFmap}[cn + r + j, j + fK] \right) \tag{2.6}$$

$$\forall f, r, c \in [0, F-1], [0, m-1], [0, m-1]$$

Followed by a lift operation on the output $\hat{OFmap}$ matrix using (2.6)

Illustration of this data transformation is presented in Figure 2.4

Pros of lowering/ lifting

Conv as GEMM Offers the most flexibility because it's insensitive to changes in convolution parameters

It also allows leaves us with a GEMM accelerator which is useful for many other NN layers e.g Linear/ Self attention/ LSTM

Con is that it still causes bloat in ifmap and additionaly complexity/ latency of lifting/ lowering. Which in the balanced case is $m^2 K$ [1]

2.4 Implementing convolutions in hardware

2.4.1 The dataflow taxonomy

In the dataflow design space, from [14] dataflows can be represented using the direct convolution nested loop structure combined with unroll pragmas. Listing 3.2 shows a generic implementation of a single convolution layer as a loop structure under a weight stationary dataflow
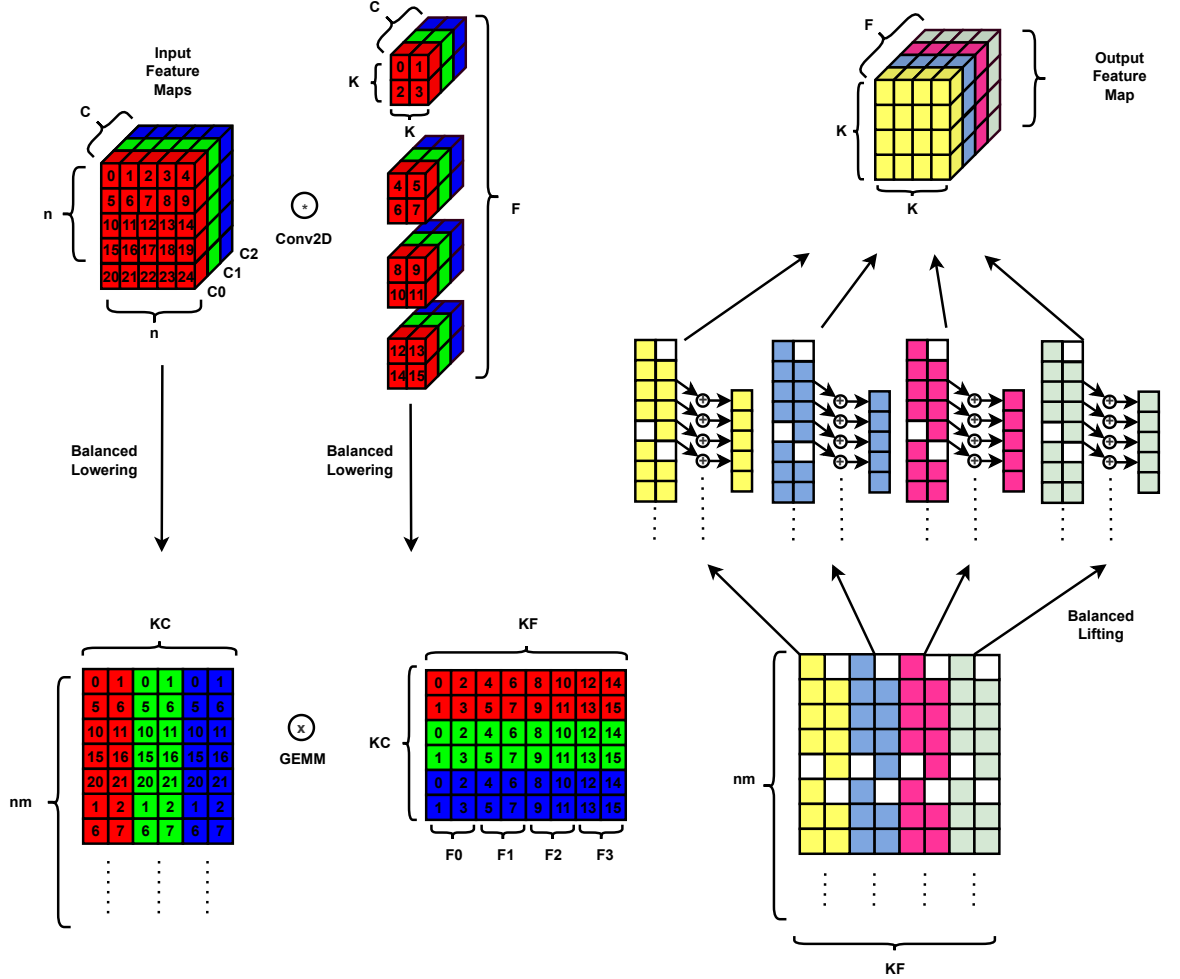
Figure 2.4: Balanced Lowering/Lifting Illustrated

configuration. What defines that dataflow is 1) loop unroll targets 2) loop order 3) the unroll factors of the unrolled loops. Weight elements within a kernel remain stationary throughout the computation of an output feature map until a new tile of channels C_T is loaded into the accelerator. Once the weights within a particular channel and filter group are used to produce an output feature map they are discarded and are only loaded again when computing the same layer for a new input image. From listing 3.2 we can see that from the loop unroll targets and loop unroll factors there are many other possible dataflow configurations available to us outside of weight stationary. Additionally, since accelerators are generally limited to two spatial axis the loops of the convolution operation

can be mapped to two spatial axis. If we allow multiple convolution loops under some kernel unroll factor KY_T/KX_T to be unrolled and mapped to the same accelerator spatial axis we can influence the effective unroll factors when performing different convolutions of different kernel sizes other than KY_T/KX_T. The choice of which loops are mapped to which spatial axis is an additional design dimension alongside loop unrolling. To summarize, from the loop representation of convolution accelerator dataflows we have three design space dimensions, 1) Loop unroll targets 2) Loop unroll factors 3) Loop spatial mapping. Given the size of this dataflow design space we will use CIGAR and Tempo to derive the common case for convolution layers and limit the scope of the dataflow design space.

CNN layer loops + loop ordering + Loop tilings can express different accelerators dataflows like row stationary, weight stationary, etc

Listing 2.2: Convolution implemented as nested loops

```
1   #pragma UNROLL F_T
2   for(int f = 0; f < F; f+=F_T) // Filter loop
3   #pragma UNROLL C_T
4       for(int c = 0; c < C; c+=C_T) // Channel loop
5   #pragma UNROLL Y_T
6           for(int y = 0; y < Y; y+=Y_T) // Output feature map row
7   #pragma UNROLL X_T
8               for(int x = 0; x < X; x+=X_T)  // Output feature map col
9   #pragma UNROLL KY_T
10                  for(int ky = 0; ky < KY; ky+=KY_T)  // Kernel row
11  #pragma UNROLL KX_T
12                      for(int kx = 0; kx < KX; kx+=KX_T)  // Kernel col
13                          O[f][y][x] += I[c][y+ky][x+kx]*W[f][c][ky][kx];
```

From dataflow we can derive hw implementation based on communication pattern and reuse behavior of the individual data elements accessed in the convolution layer.

2.4.2 The Hardware Implementation taxonomy

Figures in Figure 2.5 show different reduction/ multicast schemes based on reuse behavior of data elements (IFmap, OFmap, Weights) apparent in the dataflow. The space of available schemes is not limited to those presented in Figure 2.5 though. In [7] a hardware taxonomy illustrated in figure **??**.

Depending on the dataflow described using the dataflow taxonomy (1) loop ordering (2)
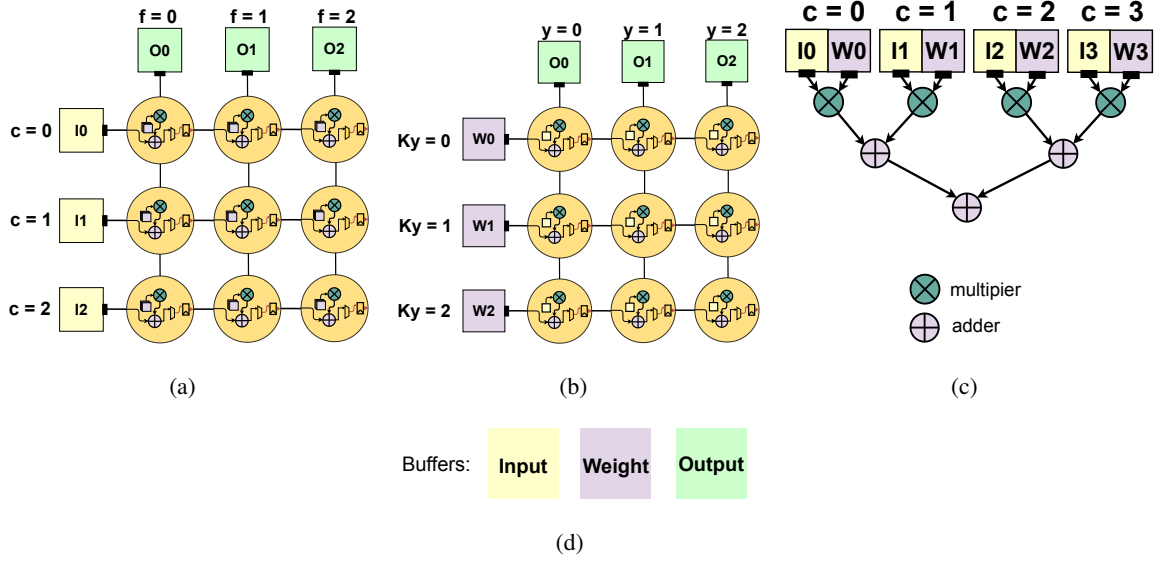
Figure 2.5: Illustration of different dataflow implementations adapted from [14] (a) blah (b) blah (c) blah (d) blah

unroll targets (2) loop unroll factors. The implementation options are derived based on the type of reuse present in the dataflow. Following the hardware implementation taxonomy presented in in [7], we can classify the available hardware implementation options based on the the type of reuse is spatial (reuse distance = 0) or temporal (reuse distance ¿ 0) that exists for a given data element accessed in the dataflow. Within a reuse type, depending on the nature of the reuse, if it is read or read modify write, there are several options for supporting the communication inferred from the reuse. To deduce the type of reuse and overall communicaiton behavior for each data element in any dataflow we can use the polyhedral model to detect temporal reuse. Spatial reuse detection can be inferred directly from the loops.

2.5 Analysis of data reuse with the polyhedral model

[8] used polyehdral model to analyse reuse within stencil based applications described as nested loops. One important element in their approach is their program written in iscc that can determine temporal reuse of data elements

There's the polyhedral extraction tool out there but unfortunately there's no way to encode parallelism or loop unrolling in it without relying on compiler pragmas.

below is an example of this reuse applied to the gemm loops
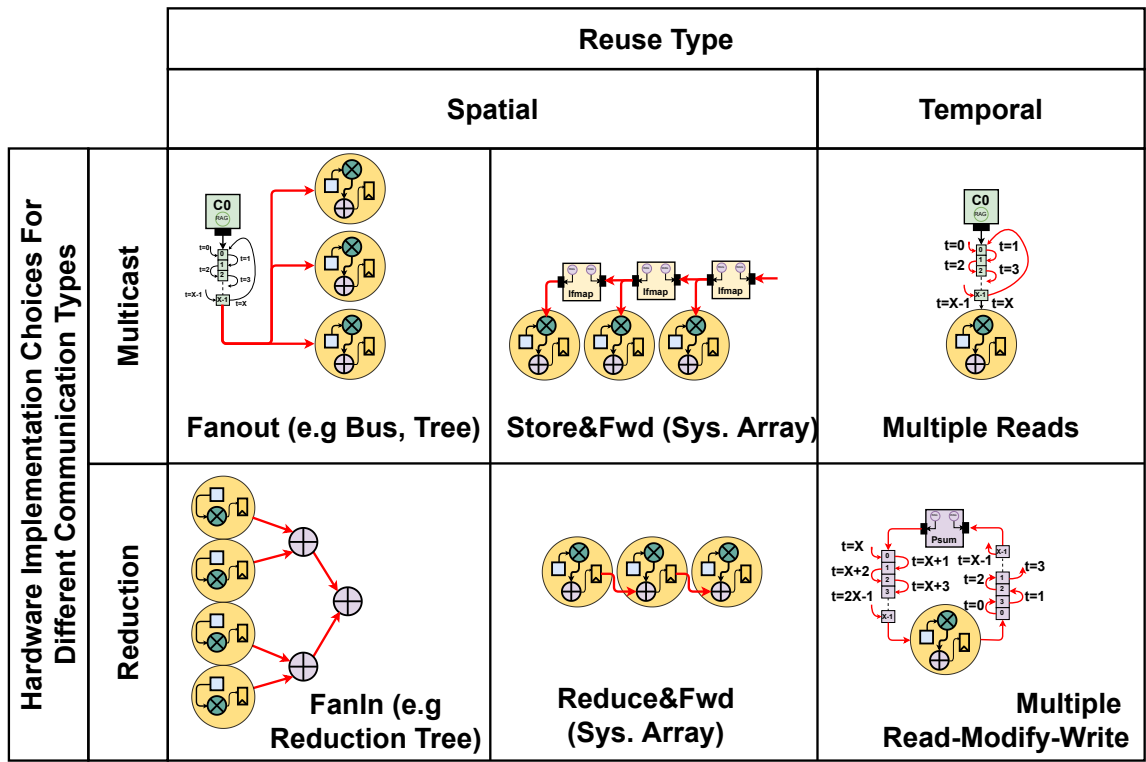
Figure 2.6: Hardware Implementation Taxonomy adapted from [7]

Chapter 3

Data-Aware Accelerator Dataflow Design Space Exploration

As discussed in chapter 2, any convolution accelerator can be reduced into it's dataflow and hardware implementation choices. Based on the dataflow exploration approach in [15] dataflows are explorable through the nested loop structure that makes up a convolution layer introduced in chapter 2. The design space dimensions of dataflows is comprised of:

- Loop ordering of the nested loops structure

- Loop unroll targets (which loops are unrolled and which are not)

- Loop unroll factors for the loop unroll targets

- Mapping of loops to an accelerators spatial axis of which there are 2

Ideally dataflow design space exploration should be hardware implementation agnostic. We can enumerate the size of the design space by examining the scope of the afformentioned design space dimensions. Beginning with the choice of loop unroll targets. One can choose to unroll only one loop or all loops with varying unroll factors. Unrolling loops exposes opportunities for parallelism when executing unrolled loops on an accelerator. Therefore the number of possible combinations of loop unroll targets is $\sum_{l=1}^{6} \binom{6}{l}$ with a total of 6! possible orderings for said loops. The space of possible loop unroll axis mappings is $\binom{l}{\min(2,l)}$ depending on the chosen number of loops l unrolled. The space of possible unroll factors is then dictated by the upperbounds of the indexes in the loop representation $max(F).max(C).max(Y).max(X).max(KY).max(KX)$

and the upperbound of the available processing engines $Count_{pe}$. Some combination of upper bounds are very unlikely to occur in real networks which limits the size of the design space for loop unroll factors. However, when considering the mapping of unrolled loops to an accelerator's spatial axis, the choice of unroll factors becomes more complicated. When two loops are unrolled in the same spatial axis, the effective unroll factor for each one of them may change when processing a layer with a different convolution layer configuration than the one assumed when unrolling the loops. For example, consider the following situation. For a convolution layer with kernel size 3x3 and channel count 32, if the kernel loops are unrolled fully with an unroll factor of 9, and the channel loops are unrolled partially with an unroll factor of 4, and they were both mapped to the same spatial axis, then the total number of processing engines allocated to that spatial axis would be 36. After allocating those PEs, if we attempt to execute a different convolution layer with a different configuration, for example, a 1x1 convolution layer with 32 channels, the allocated PEs would be underutilized because the effective channel unroll factor would be 36 instead of 4 in the original configuration.

In this chapter we will first prune the dataflow design space dimensions in section 3.1 by determining the apprioriate loop ordering and loop unroll targets and loop unroll factors using insights acquired from CIGAR a convolutional network analysis tool discussed in subsection 3.1.1. Then, given the complexity of exploring loop unroll factors and loop axis mapping, an automated accelerator Template optimizer TEMPO introduced in section 4.2 is used to explore the the afformentioned design space dimensions to produce utilization optimized accelerator template configurations.

3.1 Pruning the design space with CIGAR

3.1.1 CIGAR: The ConvolutIon statIstics GAtherer

3.1.1.1 Algorithm

Psudocode for CIGAR's algorithm is presented in algorithm 1. In algorithm 1, CIGAR begins by calling Collect_Library_Statistics after acquiring a dictionary of pytorch models $modell_{dict}$. Collect_Library_Statistics then instantiates an empty $model_{dict}^{stats}$ to be populated with model layer statistics . It then instantiates a collector object that acts as a container for collected model statistics. For each model, a new input image tensor is created based on the requirements of the model being analyzed. If no special transformations are required a default image tensor configuration is
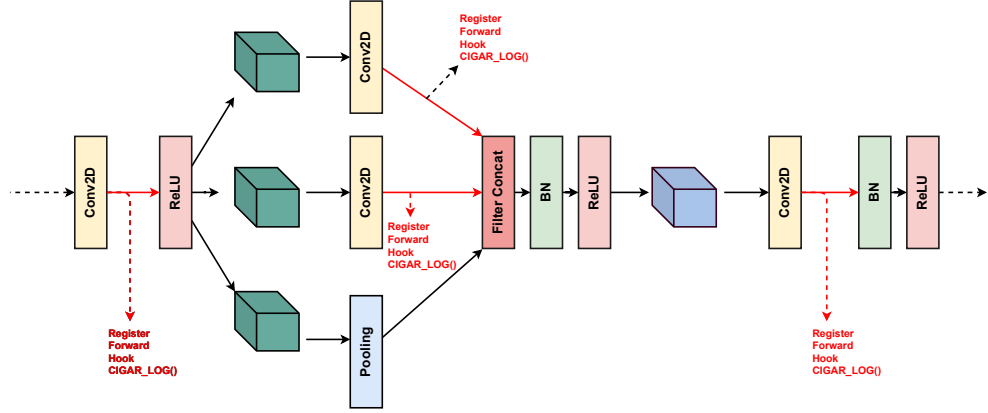
Figure 3.1: CIGAR attachment of forward hooks to all model convolution layers

used where the width and the height dimension of the image is set 224x224 with 3 RGB channels. After an image tensor is created, Attach_Collection_Hooks is called to attach the collector object's extract_stats callback function or hook on each Conv2D layer present in the model's layers. Attach_Collection_Hooks returns an array to each attached hook to be later detached once the model under inspection is processed. An illustration of this process is given in Figure 3.1.

After all forward hooks are attached to the model, a forward pass of the model is performed. Model layer statistics are added to the $model_{dict}^{stats}$ and the collector's internal layer statistics tracker is reset. The layer statistics collected are 1) the kernel sizes 2) strides 3) any additional padding 4) input/output tensor dimensionalities 5) the number of convolution groups. After processing all of the models in $model_{dict}$, a $model_{dict}^{stats}$ is returned for further analysis used to derive the necessary library insights for pruning the dataflow design space. An illustration of that process is available in Figure 3.2. New layers can be analysed by CIGAR provided that the collector is updated to be able to collect statistics from different layer types and Attach_Collection_Hooks is allowed to attach the collector's callback function to the newly supported layer.
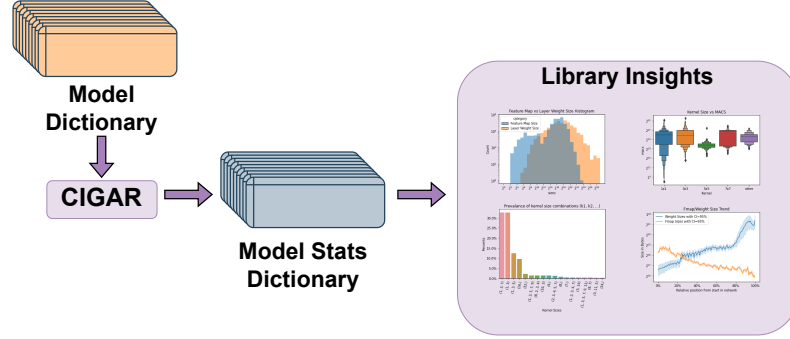
Figure 3.2: CIGAR extraction of convolution layers

Algorithm 1 CIGAR

Input: $model_{dict}$

Output: $model_{dict}^{stats}$

1: **function** ATTACH_COLLECTION_HOOKS($model, collector$)
2:      $hooks \leftarrow []$
3:      **for** $layer \in model.named\_modules()$ **do**
4:          **if** $type(layer)$ is $conv2d$ **then**
5:              $hooks.push(layer.register\_forward\_hook(collector.layer\_collector))$
6:          **end if**
7:      **end for**
8:      **return** $hooks$
9: **end function**

10: **function** COLLECT_LIBRARY_STATISTICS($model_{dict}$)
11:      $model_{dict}^{stats} \leftarrow \{\}$
12:      $collector \leftarrow Collector()$
13:      **for** $(model_{name}, model) \in model_{dict}$ **do**
14:          $input\_img\_tensor \leftarrow transform(open('default.jpg'), model)$
15:          $hooks \leftarrow Attach\_Collection\_Hooks(model, collector)$
16:          $model.forward(input)$
17:          $model_{dict}^{stats}[model_{name}] \leftarrow collector.model\_stats()$
18:          $collector.reset()$
19:          $hooks \leftarrow Detach\_Collection\_Hooks(hooks)$
20:      **end for**
21:      **return** $model_{dict}^{stats}$
22: **end function**
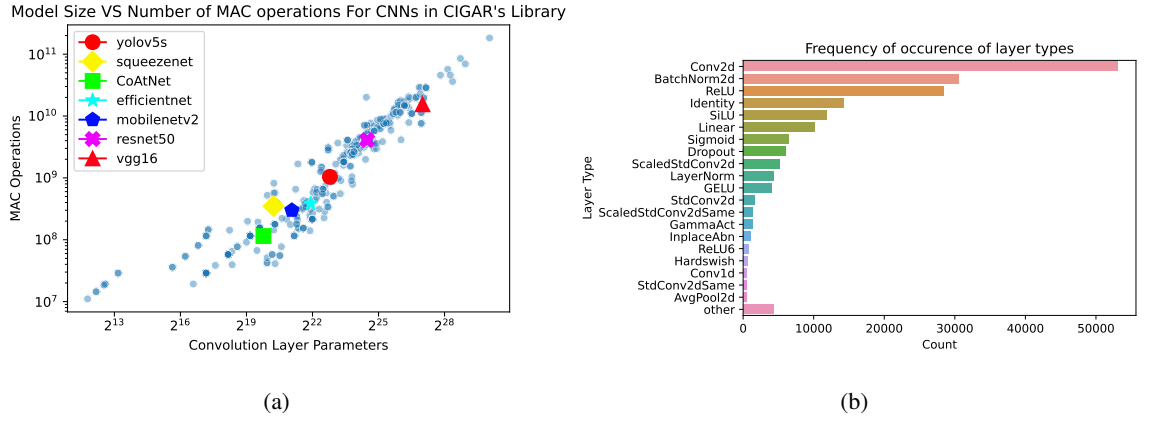
Figure 3.3: Illustration of CIGAR's library diversity based on (a) Model sizes and number of MACS (b) Model layer types

3.1.1.2 Neural Network Library Explored

A diverse range of networks were explored by CIGAR for dataflow design space pruning. The diversity of networks is reflected in the diversity of model types, layer types, model sizes, and the number of MACs in the network. An illustration of the model sizes vs number of MAC diversity is presented in Figure 3.3. From Figure 3.3 it is clear that a wide range of models were selected as part of the CIGAR library explored. The library includes smaller models like squeezenet and mobilenetv2 as well as larger models like VGG16 [10]. Additionally, in addition to image recognition networks, the library includes object detection networks like yolov5 [17]. In terms of layer diversity the library includes conventional networks with both convolution layers and linear layers as well as newer more exotic networks that combine tranformer self attention layers with convolution layers like CoAtNet [13]. An illustration of that layer type diversity is reflected in figure Figure 3.3.b. A total of 63 base networks where explored, of which there are 419 variants. The full list of networks explored is available in the appendix of this thesis. All models explored by CIGAR were implemented in pytorch and provided by either torchhub in [9] or the PyTorch Image Models (timm) package in [11].

(a)   (b)
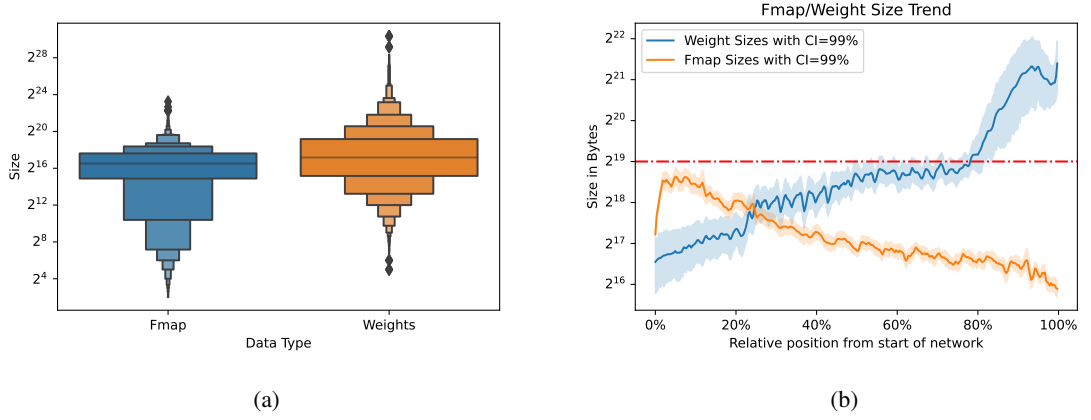
Figure 3.4: Exploration of Feature map vs Weights sizing statistics a) in entire CIGAR library b) as trends within networks

3.1.2 Applying CIGAR to prune the dataflow design space

3.1.2.1 Loop Unroll Targets

After running CIGAR on the model library referenced in subsubsection 3.1.1.1 the aggregate library statistics show that there exists a discrepancy in layer feature map sizing vs layer weight sizing as seen in Figure 3.4. While both data types share similair median sizes at 2^{17} (assuming 8 bit precision for both), for 95% of layers, IFmap sizes fell below $2^{19.11}$ bytes, but for 95% of layers weights, weight sizes falls below $2^{22.17}$ bytes. This descripency in sizing suggests that a weight stationary dataflow involving the loop unroll targets F, C, KY, and KX might be appropriate given that it maximizes on-chip reuse of weights and minimizes expensive reloads of weights from DRAM. A reduction of DRAM activity generally leads to better energy efficiency during processing of a convolution layer. Additionally, due to the overlap between 1x1 convolutions and GEMM discussed in chapter 4, the choice of a weight stationary dataflow lends itself well to GEMM given the similarities in the loop structure with regards to F and C loops for both applciations. Furthermore, a weight stationary based dataflow allows support for linear layers which are quite prevelant in many moder networks as seen in Figure 3.3.b.

Listing 3.1: Weight stationary dataflow

```
1   #pragma UNROLL F_UNROLL
2   for(int f = 0; f < F; f+=F_UNROLL) // Filter loop
3   #pragma UNROLL C_UNROLL
4       for(int c = 0; c < C; c+=C_UNROLL) // Channel loop
5           for(int y = 0; y < Y; y+=1) // Output feature map row
6               for(int x = 0; x < X; x+=1)  // Output feature map col
7   #pragma UNROLL KY_UNROLL
8                   for(int ky = 0; ky < KY; ky+=KY_UNROLL)  // Kernel row
9   #pragma UNROLL KX_UNROLL
10                      for(int kx = 0; kx < KX; kx+=KX_UNROLL)  // Kernel col
11                          O[f][y][x] += I[c][y+ky][x+kx]*W[f][c][ky][kx];
```

Listing 3.2: GEMM loops

```
1       #pragma unroll F_UNROLL
2       for(int f = 0; f < F; f+=F_UNROLL) // Filter loop
3       #pragma unroll C_UNROLL
4           for(int c = 0; c < C; c+=C_UNROLL) // Channel loop
5               for(int z = 0; z < Z; z+=1)
6                   O[f][z] += W[f][z]*I[c][z];
```

3.1.2.2 Loop Unroll Factors

There exists significant variation with regards to the kernel sizes present in CIGAR's library. This makes the question of unroll factors and axis mapping for the KY and KX loops more difficult.

From Figure 3.5.a 1x1 and 3x3 kernel sizes dominate in comparison to all other kernel sizes. This renders the choice of keeping KY and KX loops folded impractical because if support is extended to an arbitrary K x K kernel while KY and KX loops are folded the onboard storage for weights would then need to be at least K^2 where K is the upperbound of kernels supported directly to avoid excessive weight fetches from DRAM. Unfortunatly, for 60% of the layers in the network, that additional storage area would be significantly underutilized by a factor of $\frac{1}{K^2}$ due to the overrepresentation of 1x1 kernels. To mitigate this underutilization of onboard memory for weights, KY and KX loops need to be unrolled fully. However, this begs the question, what kernel sizes should be assumed when unrolling the KY and KX loops? Any kernel sizes assumed when unrolling KY and KX loops become kernel sizes that are supported directly. Kernel sizes that are

not assumed when unrolling KY and KX loops can be supported indirectly through the approach outlined in chapter 4. This means that 1x1 kernels are assumed when unrolling KY and KX loops, hence they are by definition supported directly. Other kernel sizes to support directly can be derived from Figure 3.5.

In Figure 3.5.b many networks contain at least 1 convolution layer that is not 1x1 or 3x3. For example a 7x7 kernel exists in around 37% of networks. The reason for the prevalance of 7x7 convolutions originates from the historical use of resnet [5] as a feature extractor for a significant portion of networks analyzed by CIGAR. In Figure 3.5.c, when adjusting for the the number of MACs present in layers where these kernel sizes exist, 1x1 and 3x3 kernels share a similar computational burden on the network with 1x1 having a much wider spread. 7x7 kernels have a much tighter spread but they still represent a similar computational burden to 3x3 kernels in networks where they are present. In Figure 3.5.d we can see that in networks where non 1x1 and 3x3 kernels exist, they are not likely to dominate network layers which echo's the prevalance data in Figure 3.5.a. For example the median percentage of 7x7 and 5x5 layers in a network that has them is 1.5% and 11.1% respectively. From Figure 3.5 it is clear that 1x1 and 3x3 kernels need to be supported directly while all other kernels need to be supported indirectly through the approach in chapter 4. This limits the space of possible unroll factors for the loop unroll targets and thus prunes the dataflow design space. Supporting kernels indirectly will lead to an expansion of the IFmap due to the duplication introduced by lowering, however that expansions is negligble given the scarcity of non 1x1 and 3x3 layers. Applying lowering to unsupported layers increases the required storage for IFmap due to lowering from from $2^{19.11}$ to at most $2^{19.25}$ for 95% of layers.

(a)

(b)

(c)

(d)
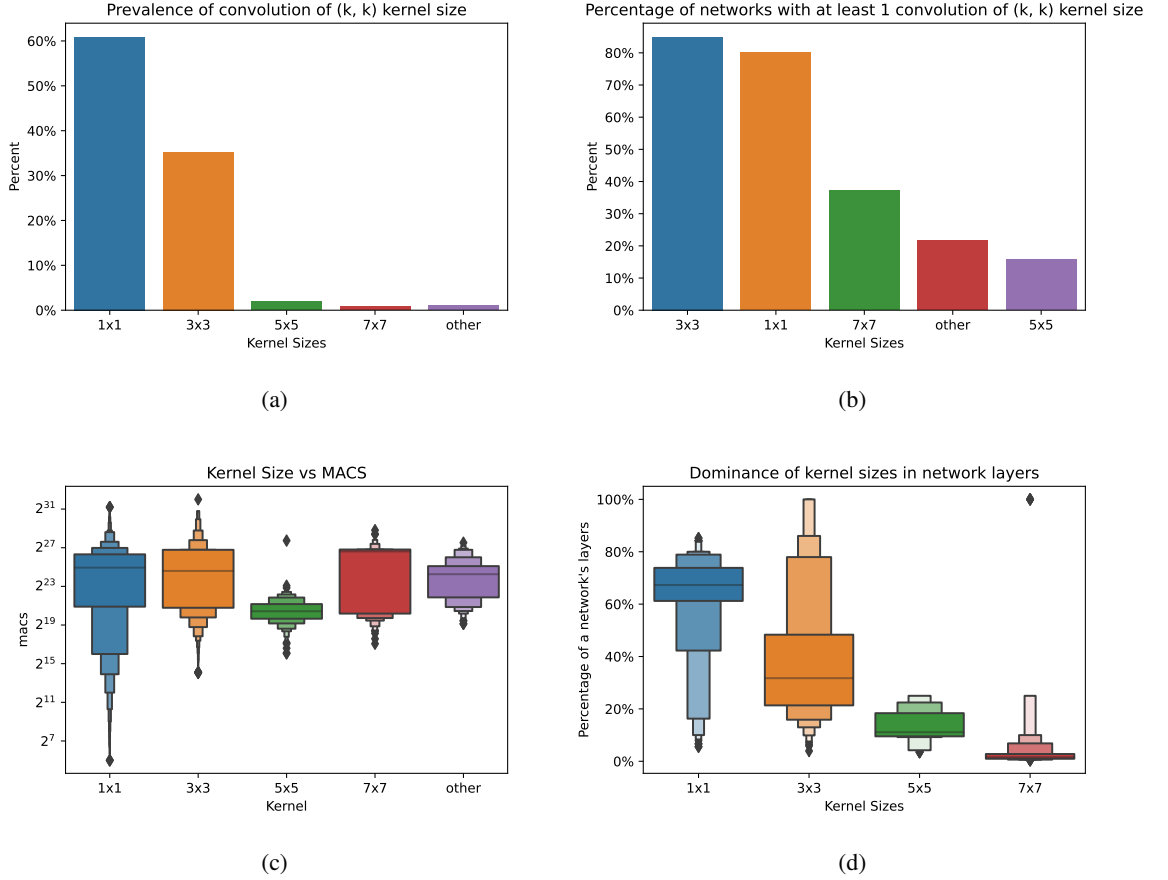
Figure 3.5: Feature map vs Weights sizing statistics in (a) Entire CIGAR library (b) For each convolution layer in the network

Depending on the chosen unroll factors, the architecture implementing the unroll factors in effect tiles the weight tensor and processes it tile by tile in the convolution operation. An illustration of this concept is present in Figure 3.6. Loop unroll factors determine PE allocation Tiling of a weight tensor arises from the processing of filters, channels and kernels in chunks whose size depend on the unroll factors. Padding of a weight tensors is performed wherever the chosen PE binding for filter or channel loops exceeds the number of channels and filters being processed in the tile. In Figure 3.6 a weight tensors of dimension $R^{6\times3\times2\times2}$ is tiled with $F_{unroll} = 4$, $C_{unroll} = 8$, $K_{unroll} = 2$ with kernel loops mapped to the horizontal axis alongside channel loops. Additional padding in the horizontal and verticle axis is added given excess allocation of PEs in both spatial axis in all tiles except the top left one. This representation of the weight tensor as a series of tiles
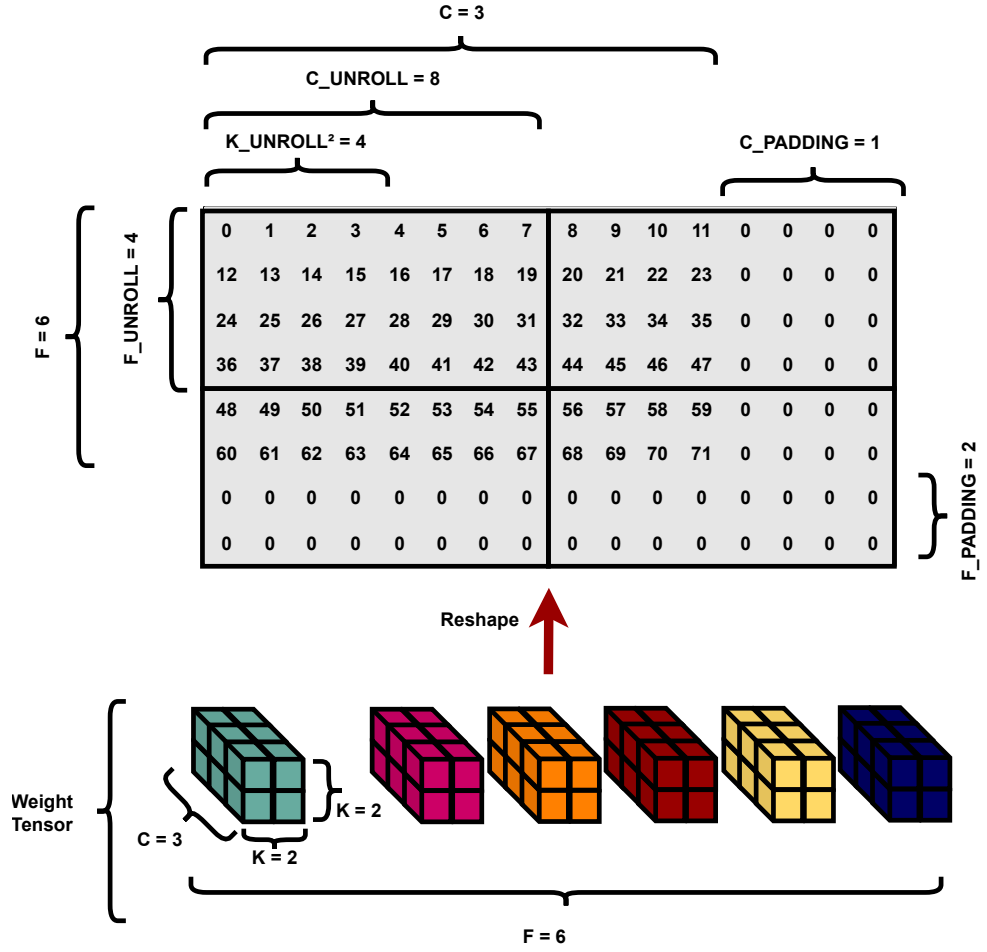
Figure 3.6: GEMM and 1x1 Convolution Equivelence

processed by the architecture is useful when considering different schedules for processing weights. A discussion of tile scheduling is given in the next section.

3.1.2.3 Loop ReOrdering

While a weight stationary offers limited flexibility with regards to loop reoredering it does offer some degree of flexibiltiy with regards to ordering filter loops and channel loops. F, C loop ordering affects required on-chip storage for IFmaps and OFmaps. Under Direct mode and Gemm mode with balanced lowering, IFmap sizes do not exceed $2^{19.25}$ bytes (assuming 8 bit precision) for 95% of all convolution layers in CIGAR's library. An estimation of the on-chip area required to store IFmaps using the model presented in [4] yields a total on-chip area per sram bit stored equal to 0.013 um^2 which translates to $0.064mm^2$ on-chip area dedicated to sram buffers for storing entire input feature maps for a layer at 14nm technology. This area/storage does not scale with increased/decreased filter unroll factor, channel unroll factor or max directly supported kernel size. On-Chip area dedicated to storing Weights scales with the afformentioned parameters. Storage with regards to OFmaps depends on the loop ordering in the chosen dataflow. Specifically on-chip OFmap storage depends on whether filter loops and channel loops are reordered such that OFmaps are retired as fast as possible (ASAP tile scheduling) by iterating through IFmap channels first while processing a groups of filter, or as late as possible (ALAP tile scheduling) by iterating through filters first while processing a group channels. These two orderings for filter loops and channel loops represent different tile schedules for processing convolution layers. An illustration of both tile scheduling approaches is illustrated in Figure 3.8. In Figure 3.8 a 1x1 convolution layer's weights are shown with the architecture's unroll factors overlayed on top. The overlay of the architecture's unroll factor creates distinct weight tiles where componenets of the OFmap are computed. The order of executing these weight tiles depends on the chosen tile schedule. ASAP which represents F, C loop ordering and ALAP which represents C, F loop ordering.

A tradeoff between required IFmap storage and required OFmap storage is apparent in ??. Under ASAP scheduling, storage requirements for OFmaps scales with F_{unroll} because F_{unroll} represents the maxmimum number of filters in flight. Storage requirements for IFmaps is maximized under ASAP because all channel data would need to be held on-chip assuming no additional reads can be made from DRAM for IFmap channels. Under ALAP scheduling, storage requirements for IFmap scale with C_unroll because C_{unroll} represents the maximum number of channels in flight. Storage for OFmaps is maximized under ALAP. In this thesis it is assumed that chip area (and thus on-chip memory) is always sufficient at least one of the afformentioned tile schedules without requiring loop blocking and additional DRAM accesses for feature maps. An exploration of the effect of loop blocking under more restrictive area constraints is relegated to future work.

(a)   (b)
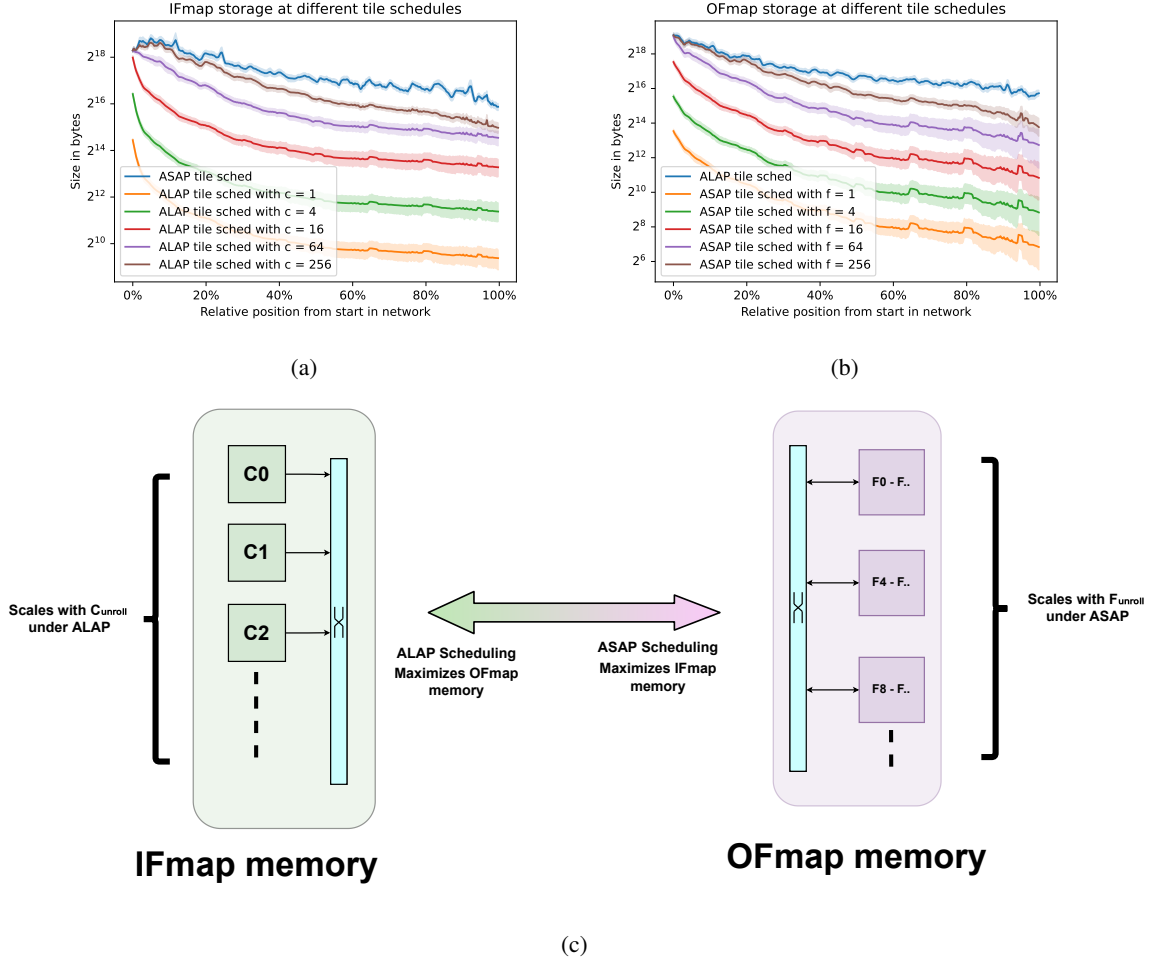

(c)

Figure 3.7: Illustration of storage tradeoff between OFmaps and IFmaps depending on tile scheduling (loop ordering) and accelerator template parameters (loop unroll factors) (a) IFmap storage (b) OFmap storage (c) archictural illustration
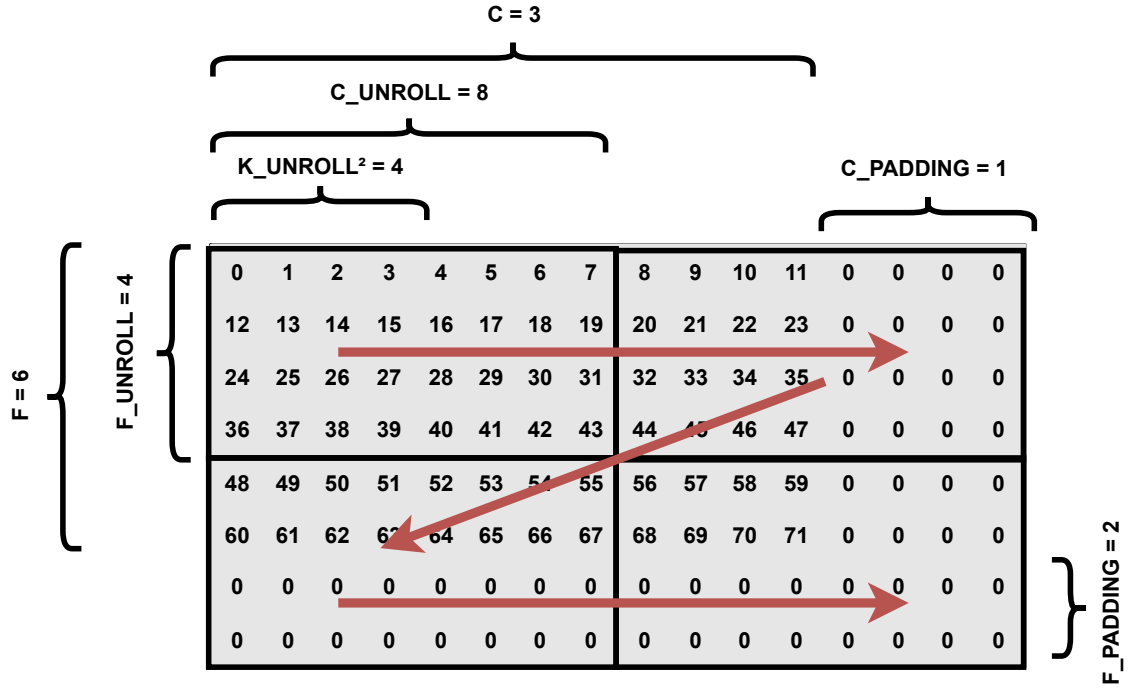
(a)
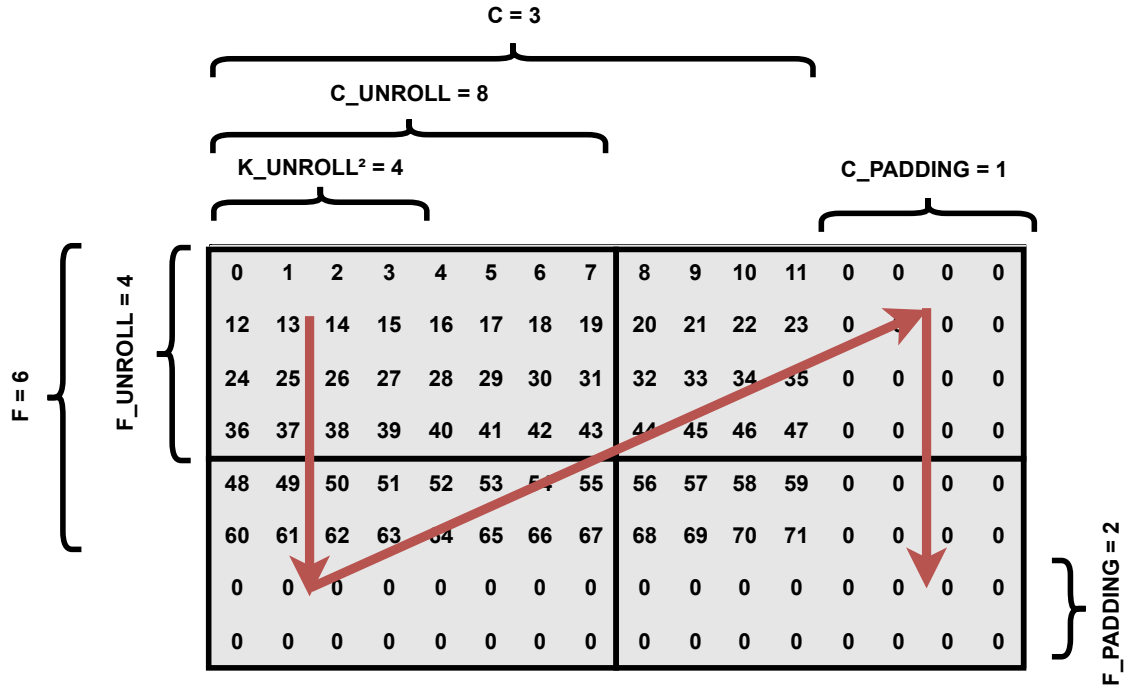
(b)

Figure 3.8: Illustration of different tiling schedules (a) ASAP scheduling (F, C) (b) ALAP scheduling (C, F)

26

3.2 Hardware Implementation design space exploration with the Polyhedral Model

Based on the conclusion derived from chapter 3, the ideal conv. accelerator operates in two modes, direct Mode where 3x3 kernel with stride 1 are supported and GEMM mode where all other kernel sizes and strides are supported in GEMM mode via the approach in (REFERENCE LOWERING/ LIFTING CHAPTER). In this section we will deduce the optimal hardware implementation for the weight stationary dataflow chosen in chapter 3 by analyzing data reuse in the loop based representation of the aforementioned dataflow. To perform this deduction we will use the polyhedral model to analyse temporal reuse in subsection 3.2.1 and spatial reuse in subsection 3.2.2. Finally, in subsection 3.2.3 a simplification of the IFmap memory hierarchy present in the optimal hardware implementation derived in subsection 3.2.1 and subsection 3.2.2 is presented.

3.2.1 Temporal Reuse Analysis

Unrolling convolution dataflow loops yield multiple instances of the Multiply and Accumulate (MAC) statement present in the original convolution nested loops in Listing 3.1. These instances will be referred to as MAC spatial instances to distinguish them from temporal instances discussed in this chapter. MAC spatial instances can be distinguished based on the memory access offsets that exist in them as a result of unrolling filter, channel and kernel loops. For unroll factors F_T for filters, C_T for channels, KY_T and KX_T for kernels each statement will have a coresponding access offset based on the spatial instance index $j \in [0, F\_T * C\_T * KY\_T * KX\_T]$ for each of the data elements (IFmap, OFmap and Weights) accessed in the loop body. Each MAC spatial instance at index j is characterized by a set of access offsets Fj, Cj, KYj, KXj used by the memory accesses in the MAC statement. Applying the unroll factors and distinguishing each MAC statement based on it's statement index j yields the loop configuration in Listing 3.3.

Listing 3.3: Fully unrolled convolution dataflow loops

```
1       for(int f = 0; f < F; f+=F_T) // Filter loop
2           for(int c = 0; c < C; c+=C_T) // Channel loop
3               for (int y = 0; y < Y; y++) // FeatureMap Height
4                   for(int x = 0; x < X; x++) // FeatureMap Width
5                       ...
6                       /* For all j in [0, F_T*C_T*KY_T*KX_T[ */
7                       O[f+Fj][y][x] += W[f+Fj][c+Cj][KYj][KXj]* \
```

```
8                                                      I[c][y+KYj][x+KXj]
9                               . . .
```

Temporal reuse analysis is performed on the above loops. The different operational modes (GEMM/ Direct) are analysed concurrently using the same loop representation below as they only differ based on whether we fuse feature map height and width loops, and set upper bounds of the kernel loops to 1. Since kernel loops are always unrolled fully this sets KY_T and KX_T to 1. We can analyse temporal reuse in the dataflow represented in Listing 3.3 by adapting the approach in [8] to the afformentioned dataflow iteration domain and access functions. Given iteration domain restrictions imposed by the polyhedral model, Listing 3.4 assumes unroll factors F_T = C_T = 4. Setting F_T and C_T to concrete values does not affect output results of temporal reuse analysis.

Listing 3.4: Polyhedral analysis of reuse in iscc for convolution loops

```
1    // Define iteration domain for all accessed data elements
2    ID:=[F, C, Y, X] -> { S[f, c, y, x] : 0<=f<F and 0<=c<C and f mod 4=0 and c
         mod 4=0, 0<=y<Y and 0<=x<X};
3    // Define access functions for each data element
4    IFMAP:=([Cj, KYj, KXj] -> {S[f, c, y, x] -> IF[c+Cj][y+KYj][x+KXj]})*ID;
5    OFMAP:=([Fj] -> {S[f, c, y, x] -> PS[f+Fj][y][x]})*ID;
6    WEIGHT:=([Fj, Cj, KYj, KXj] -> {S[f, c, y, x] -> W[f+Fj][c+Cj][KYj][KXj]})*
         ID;
7    // Evaluate temporal reuse
8    IFMAP_REUSE:=(IFMAP.(IFMAP^-1))*(ID<<ID);
9    OFMAP_REUSE:=(OFMAP.(OFMAP^-1))*(ID<<ID);
10   WEIGHT_REUSE:=(WEIGHT.(WEIGHT^-1))*(ID<<ID);
```

In Listing 3.4, the iteration domain for the loops in Listing 3.3 is converted into it's set representation in line 2 where for some access statement S the loop iteration vector [f, c, y, x,] is bound by the upper and lower bounds [0, F], [0, C], [0, Y], [0, X] respectively. These bounds are represented by the associated parameters passed to the iteration domain set assignment in line 2. Each memory accessed in the body of the loop has an access function at each level of that memory's hierarchy. As a result, each instance of the loop iteration vector [f, c, y, x] is mapped to a memory access for each of the memories in lines 4-6. Access offsets used in the memory access functions are passed as parameters based on the convention established in Listing 3.3. This mapping creates multiple temporal instances for each memory access in each MAC spatial instance. For example, for some iteration vector [f = 1, c = 1, y = 0, x = 1], the OFmap access that occurs at iteration vector [f = 2, c= 1, y = 0, x = 1] is a different temporal instance of the same OFmap access at [f = 1, c = 1, y = 0, x = 1]. Two accesses that access the same index but at different iteration vectors are different temporal instances of the same access. After applying the operation in lines 8-10, we can determine the temporal reuse behavior of the accessed memories in the convolution loops. Listing 3.5 shows the reuse behavior for each memory. Original iteration domains constraints are ommited for brevity.

Listing 3.5: Polyhedral analysis results w.r.t data elements in convolution loops

```
1    IFMAP_REUSE;
2    [F, C, Y, X, Cj, KYj, KXj]->{
3        S[f, c, y, x] -> S[f', c' = c, y' = y, x' = x] :
4            ... f' > f and 0 <= f' < F ...
5        }
6    OFMAP_REUSE;
7    [F, C, Y, X, Fj]->{
8        S[f, c, y, x] -> S[f' = f, c', y' = y, x' = x] :
9            ... c' > c and 0 <= c' < C ...
10        }
11    WEIGHT_REUSE;
12    [F, C, Y, X, Fj, Cj, KYj, KXj] -> {
13        S[f, c, y, x] -> S[f' = f, c' = c, y', x'] :
14            ... y' > y and 0 <= y' < Y and 0 <= x' < X ...;
15        }
```

Listing 3.5 shows the temporal reuse behavior in memory accesses. For each of the memories accessed (IFmap, OFmap and Weights) there exists a set of reuse (IFMAP_REUSE, OFMAP_REUSE and WEIGHT_REUSE) maps that map each iteration vector of an access to all the proceeding iteration vectors where that same access occurs. From the above listing we can see that, in the set of IFmap reuse maps (IFMAP_REUSE), IFmap channels are reused temporally with respect to filter loops. For a given IFmap accessed at channel c, that channel is accessed again when computing the output for all proceeding filter loop iterationtions f' where $f' > f$. The absence of other mappings in the set of reuse maps IFMAP_REUSE shows that 1) this reuse behavior holds at any arbitrary iteration vector [f, c, y, x] and 2) this reuse behavior depends only on the filter loop. For the set OFmap reuse maps (OFMAP_REUSE), for an OFmap acceess at iteration vector [f, c, y, x], it is accessed again at loop iteration f'=f, c', y'=y, x'=x where $c' > c$. For (WEIGHT_REUSE) Weights exhibit temporal reuse w.r.t feature map width and height, the X and Y loops.

Applying the hardware taxonomy in [7], IFmap exhibits temporal reuse, multicast communication. OFmap exhibits temporal reuse, reduction communication given their read-modify-write behavior. Weights exhibit temporal multicast communication. Given the limited implementation options derivable from temporal reuse we can comfortably define the appropriate connectivity and memory hierarchies for IFmaps channels, OFmaps channels (equivelent to number of Filters), and Weights. The beginings of a hardware template derived from the afformentioned temporal reuse behavior of the different memories referenced in the convolution dataflow can be seen in 3.9. In 3.9
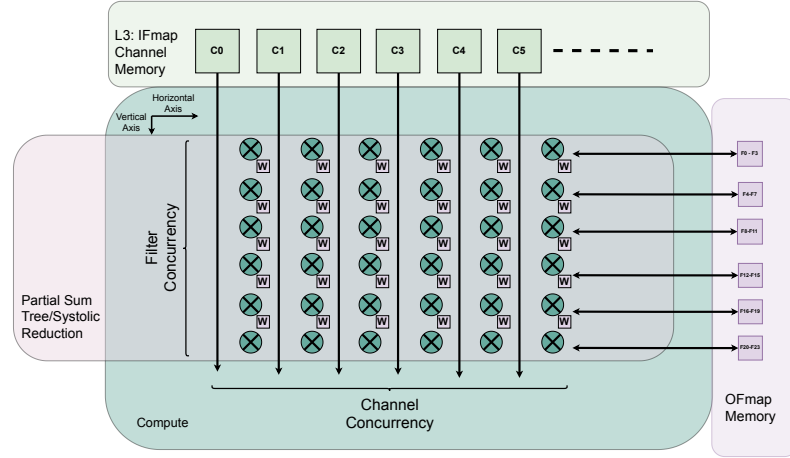
Figure 3.9: Initial hardware template incorporating buffers IFmap and OFmap temporal reuse

the template is broken into 3 major componenets. The first is the IFmap memory hierarchy currently with only 1 level. The 2nd component is the compute portion of the template where partial sums are computed and aggregating into OFmap data elements. Finally the 3rd component which is the OFmap memory that stores OFmap partial sums until they are aggregated into OFmap pixels and are written back to memory.

In addition to the temporal reuse behavior exhibited across IFmap channels, temporal reuse exists within individual IFmap channels due to the stencil based access pattern arising from the X, Y, KY, KX loops in the dataflow. That temporal reuse is affected by the decision to fully unroll kernel loops which causes temporal reuse to exist between unrolled IFmap kernel ports. Proof of the existence of that temporal reuse is given in the polyhedral analysis in Listing 3.6.

Listing 3.6: Analysis of IFmap channel reuse

```
1    ID_XY:=[Y, X, KY, KX] -> { S[y, x, ky, kx] : 0<=ky<KY and 0<=kx<KX and 0<=y<
         Y and 0<=x<X};
2    IFMAP_XY:=({S[y, x, ky, kx] -> IF[y+ky][x+kx]})*ID;
3    IFMAP_REUSE_XY:=(IFMAP_XY.(IFMAP_XY^-1))*(ID_XY<<ID_XY);
4    IFMAP_XY_REUSE;
5    [Y, X, KY, KX] -> {
6        S[y, x, ky, kx] -> S[y', x', ky' = (y - y') + ky, kx' = (x - x') + kx] :
7            ... y' > y and (y + ky) -KY < y' <= (y + ky) and (x + kx) -KX < x'
                <= (x + kx) ...;
8    }
```

31

Verticle Reuse   **Horizontal Reuse**
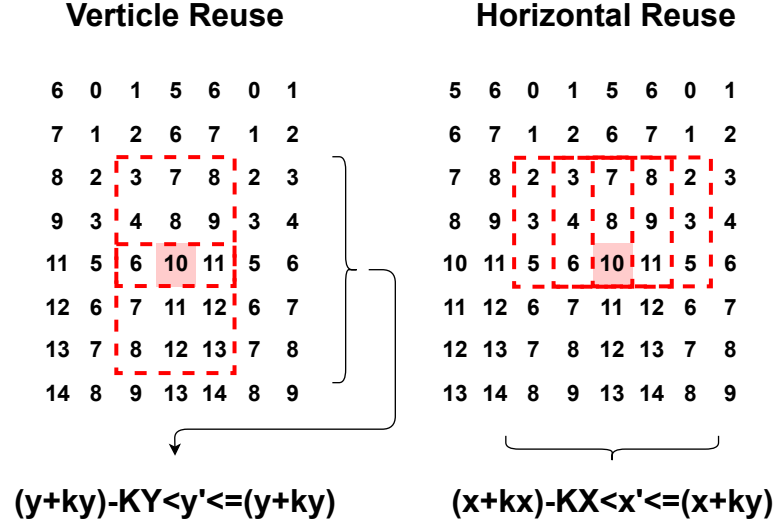
Figure 3.10: IFmap Reuse Behavior w.r.t individual feature map channels

Within an individual IFmap channel, temporal reuse is exhibited w.r.t X and Y loops. Given the complexity of the domain constraints of IFMAP_XY_REUSE in Listing 3.6, an illustration of the reuse behavior is available in Figure 3.10. In Figure 3.10, individual pixels within the kernel are reused based on the position of the sliding window or stencil of the convolution in an IFmap channel. There are two primary directions where that reuse is exhibited, vertical and horizontal with an IFmap channel. The loops that control the verticle and horizontal stencil position in the IFmap are the Y and X loops in the dataflow. Because kernel loops are fully unrolled, the temporal reuse exhibited in Listing 3.6 occurs accross unrolled kernel loop ports. To determine the appropriate memory infrastructure to support that stencil based access pattern, we can apply the technique in [8] to construct a reuse chain that moves reused data between urnolled kernel ports. The advantage of using a reuse chain is that the temporal reuse that exists within an IFmap channel is relegated to a smaller memory with lower memory access cost.

[8] constructs a reuse chain for applications with a sliding window access pattern that connects each unrolled kernel port with it's neighbors using a FIFO or a shift register. If the temporal reuse distances between the accesses of neighboring ports are constant [8] uses a shift register, otherwise they use a FIFO. The reuse distance between accesses of neighboring ports are then converted into storage of the same size. So if two ports share the same data but with a lag of 2 iterations in the iteration domain they're operating in, then a shift register of size 2 can be placed

between them. Similar to the sliding window application explored in [8] the reuse distances between the unrolled kernel ports in the convolution dataflow are also constant. To determine the reuse distances necessary between ports we can apply the analysis in Listing 3.7 adapted from [8] to determine the sizing of the buffers in the reuse chain for IFmap accesses within a channel. The analysis in Listing 3.7 assumes a kernel size of 3x3.

Listing 3.7: Determining buffer sizes in 3x3 convolutions

```
1    ID:=[IFMAP_Y, IFMAP_X] -> {S[y,x]:y>=0 and x>=0 and y<=IFMAP_Y-3 and x<=
          IFMAP_X-3};
2    A0:=[IFMAP_Y, IFMAP_X] -> {S[y,x]->A[y+0,x+0]}*ID;
3    A1:=[IFMAP_Y, IFMAP_X] -> {S[y,x]->A[y+0,x+1]}*ID;
4    A2:=[IFMAP_Y, IFMAP_X] -> {S[y,x]->A[y+0,x+2]}*ID;
5    A3:=[IFMAP_Y, IFMAP_X] -> {S[y,x]->A[y+1,x+0]}*ID;
6    ...
7    A8:=[IFMAP_Y, IFMAP_X] -> {S[y,x]->A[y+2,x+2]}*ID;
8
9    R10:=(lexmin ((A1.A0^-1)*(ID<<ID)));
10   R21:=(lexmin ((A2.A1^-1)*(ID<<ID)));
11   R32:=(lexmin ((A3.A2^-1)*(ID<<ID)));
12   ...
13   R87:=(lexmin ((A8.A7^-1)*(ID<<ID)));
```

In Listing 3.7, the iteration domain for the YX loops are defined as functions of the IFmap dimensions passed as parameters (line 1). The unrolled kernel loop IFmap accesses are then described using access maps that map the iteration vector [y,x] to the associated IFmap access (lines 2-7). Notice that the accesses are described as constant offsets added to access iterators y and x. These constants represent the kernel loop iterators ky, and kx that are now unrolled. For each neighboring pair of ports accessing the IFmap we can determine the reuse behavior in (lines 9-10). Operations in lines (9-13) map iterations where a port accesses a data element in IFmap with the earliest next iteration in which the neighboring port accesses that same data element. The distance between the accesses is then used as the reuse buffer size. The results of the analysis are presented in Listing 3.8.

Listing 3.8: Polyhedral analysis of reuse in iscc for convolution loops

```
1   R10;
2   $1 := [IFMAP_Y, IFMAP_X] -> {
3       S[y, x] -> S[y' = y, x' = 1 + x] :
4           0 <= y <= -3 + IFMAP_Y and 0 <= x <= -4 + IFMAP_X
5   }
6   R21;
7   $2 := [IFMAP_Y, IFMAP_X] -> {
8       S[y, x] -> S[y' = y, x' = 1 + x] :
9           0 <= y <= -3 + IFMAP_Y and 0 <= x <= -4 + IFMAP_X
10  }
11  R32;
12  $3 := [IFMAP_Y, IFMAP_X] -> {
13      S[y, x] -> S[y' = 1 + y, x' = -2 + x] :
14          0 <= y <= -4 + IFMAP_Y and 2 <= x <= -3 + IFMAP_X
15  }
16  ...
17  R87;
18  $8 := [IFMAP_Y, IFMAP_X] -> {
19      S[y, x] -> S[y' = y, x' = 1 + x] :
20          0 <= y <= -3 + IFMAP_Y and 0 <= x <= -4 + IFMAP_X
21  }
```

In 3.8, reuse distances between neighboring ports depend on the relationship between the ports and whether their access offsets are in the same row of the stencil or not. If two neighboring ports have unequal ky offsets the reuse distance between them is IFMAP_X-3. If two neighboring ports have an equal ky offset the reuse distance is 1. An example of the first case is lines 11-15 where the reuse distance between port 2 and port 3 is IFmap-3. The evidence of that is that for any data accessed at port 3 with iteration vector y, x that same data is accessed at port 2 at iteration vector [y+1, x-2]. Based on the lexicographic ordering of iteration vector [y, x] and [y+1, x-2], the distance between those two vectors is IFMAP_X-3, or in terms of OFmap dimensions X-1. Applying the same analysis to two ports in the same row (R10, R21, R45, R87, ...) yields a reuse distance of 1 as evidence by the iteration vectors of access [y, x] and [y, x+1] in all of the afformentioned neighboring port pairs.

Applying the results of the analysis in Listing 3.8 with the previous template Figure 3.9 results in the updated template Figure 3.11.
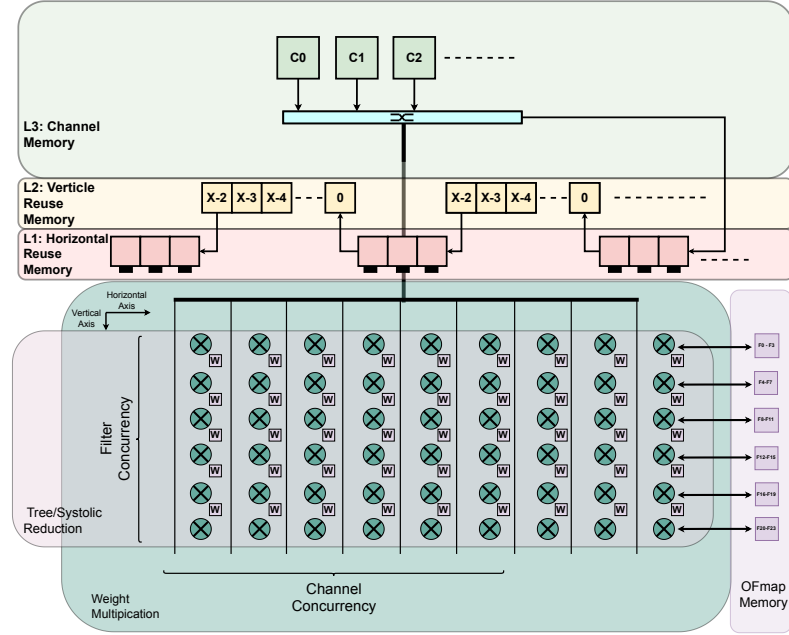
Figure 3.11: Hardware template incorporating a reuse chain for reuse within an IFmap channel

3.2.2 Spatial Reuse Analysis

So now we know the hierarchy needed to express X and Y reuse in IFmap. Applying the unroll factors in the target loops in the dataflow will yield a loop structure similar to the one in 3.9. Using the convention established in 3.2.1, each MAC statement in the unrolled loop body has an associated j index. In the loop body there exists duplicate memory accesses across individual MAC spatial instances. Those duplicate accesses are highlighted in Listing 3.9 and they are the origin of spatial reuse in the dataflow. IFmaps exhibit spatial reuse with multicast communication w.r.t to filter loops. OFmap exhibit spatial reuse with reduction communication w.r.t to channel loops. Weights exhibit no spatial reuse

Listing 3.9: Spatial reuse in fully unrolled kernel loops

```
1   for(int f = 0; f < F; f+=F_T) // Filter loop
2       for(int c = 0; c < C; c+=C_T) // Channel loop
3           for (int y = 0; y < Y; y++) // FeatureMap Height
4               for(int x = 0; x < X; x++) // FeatureMap Width
5               {
6                   O[f+0][y][x]  += W[f+0][c+0][0][0] * \
7                                       I[c+0][y+0][x+0] ; // j=0
8                   O[f+0][y][x]  += W[f+0][c+0][0][1] * \
9                                       I[c+0][y+0][x+1] ; // j=1
10                  O[f+0][y][x]  += W[f+0][c+0][0][2] * \
11                                      I[c+0][y+0][x+2];   // j=2
12                  O[f+0][y][x]  += W[f+0][c+0][1][0] * \
13                                      I[c+0][y+1][x+2];   // j=3
14                  ...
15                  O[f+1][y][x]  += W[f+1][c+0][0][0] * \
16                                      I[c+0][y+0][x+0] ; // j=C_T*KY_T*KX_T
17                  O[f+1][y][x]  += W[f+1][c+1][0][1] * \
18                                      I[c+0][y+0][x+1] ; // j=C_T*KY_T*KX_T+1
19                  ...
20                  O[f+F_T-1][y][x] += W[f+F_T-1][c+C_T-1][KY_T-1][KX_T-1] * \
21                                      I[c][y+KY_T-1][x+KX_T-1];
22                                          // j=F_T*C_T*KY_T*KX_T-1
23
24              }
```

Applying the taxonomy in Figure 7.2 to data elements that are spatially reused, IFmap channels that are spatially reused across unrolled filter loops can be broadcast with a bus. The reuse chain discussed in subsection 3.2.1 can be thought of as a Store&Forward scheme to deliver individual IFmap channel data elements to the Processing Engine (PE)s for reduction into OFmaps.Weights reused for channel iteration and are discarded. They exhibit no spatial reuse, just temporal. Therefore they should be kept in small on chip buffers, preferably close to the computation they are used in. OFmap exhibit spatial reuse across concurrent channels as well as temporal reuse across channel sets as discussed in subsection 3.2.1. A reduction tree as in Figure 3.12.a or a systolic array reduce and fwd as in Figure 3.12.b are both possible assuming no restrictions arising from synthesis. Combining the reuse chain derived in subsection 3.2.1 with the required systolic delays yields a simplification to the L1 memory present in Figure 3.11. This simplification is discussed in subsection 3.2.3.
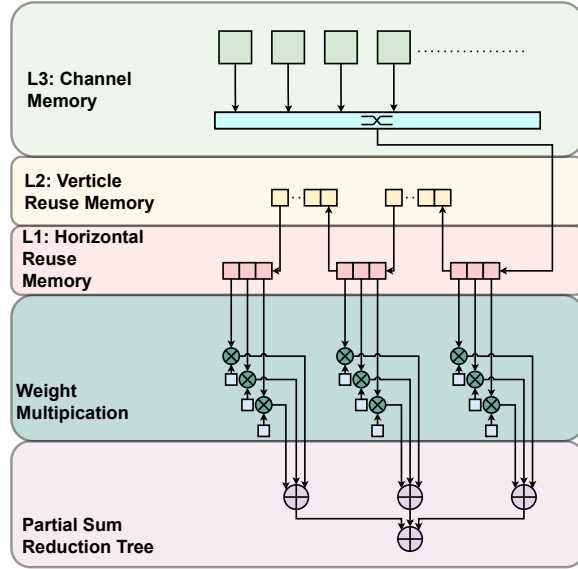
(a)
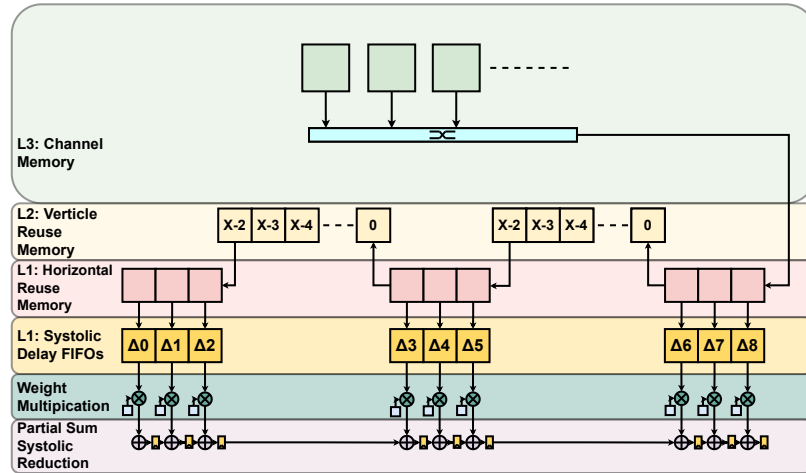
(b)

Figure 3.12: Illustration of different partial sum reduction styles assuming kernel size is 3x3 (a) Tree Reduction (b) Systolic array reduction
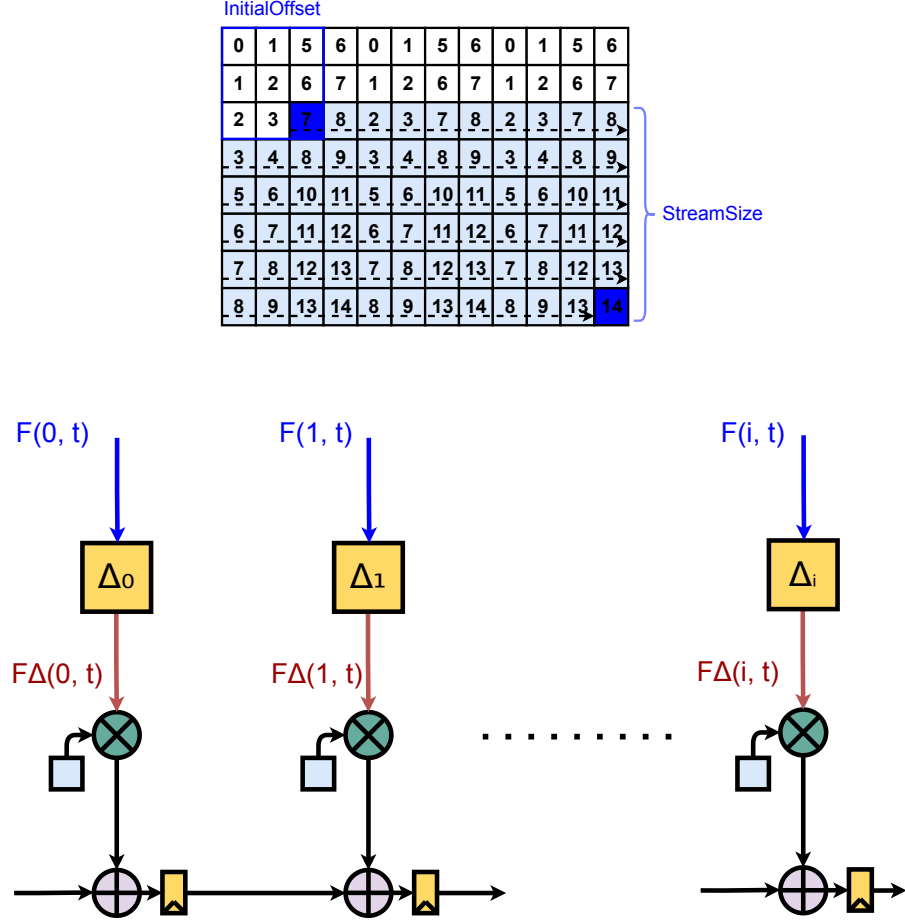
Figure 3.13: Reinterpretation of IFmap memory hierarchy outputs as a stream function

3.2.3 Simplifying the memory hierarchy

We can reinterpret the accesses made by the IFmap memory hierarchy in Figure 3.11 as a stream function $F(i, t)$ whose output produces element from an IFmap channel. The variable i is the port index of IFmap hierarchy and t is the time in cycles since the beginning of the convolution operation. A representation of this reinterpretation of the accesses made in the IFmap memory hierarchy can be seen in Figure 3.13. Since it's always assumed that in direct mode kernel loops are unrolled fully the number of ports into the IFmap memory hierarchy is always a multiple of K^2 where K is the size of the kernel being processed in direct mode.

$$IFmap \in R^{C \times n \times n} \xrightarrow{Reshape} IFmap \in R^{1 \times Cn^2} \tag{3.1}$$

$$Weight \in R^{F \times C \times K \times K} \tag{3.2}$$

$$F(i, t) = \begin{cases} IFmap_{A(i,t)} & 0 <= t < StreamSize \\ 0 & else \end{cases} \tag{3.3}$$

$$StreamSize = n(n - K) + (n - K) \tag{3.4}$$

$$A(i, t) = InitialOffset(i) + t \tag{3.5}$$

$$\tag{3.6}$$

Each data element streamed from the IFmap depends on the an access function that also takes the same variables i and t. Depending on the port index i the access function for each port is composed on an initial offset in the IFmap and the current cycle count. The number of cycles in which output from the IFmap memory hierarchy can be produced is limited to the stream size of the IFmap currently being processed. The stream size is a function of the IFmap dimensions and the kernel Size.

$$InitialOffset = C_i n^2 + Y_i n + X_i \tag{3.7}$$

$$C_i = \lfloor \frac{\lfloor \frac{i}{K} \rfloor}{K} \rfloor \tag{3.8}$$

$$Y_i = (\lfloor \frac{i}{K} \rfloor) \bmod K \tag{3.9}$$

$$X_i = i \bmod K = (i - \lfloor \frac{i}{K} \rfloor K) \tag{3.10}$$

$$\tag{3.11}$$

The initial offset function defines the initial index offset in the IFmap the stream starts from for each port i. It can be decomposed into three main offsets. A channel offset C_i, a row offset Y_i and a column offset X_i.

$$F_\Delta(i, t) = \begin{cases} IFmap_{A_\Delta(i,t)} & \Delta_i <= t < \Delta_i + StreamSize \\ 0 & else \end{cases} \tag{3.12}$$

$$\Delta_i = i \tag{3.13}$$

$$A_\Delta(i, t) = A(i, t) - \Delta_i \tag{3.14}$$

$$\tag{3.15}$$
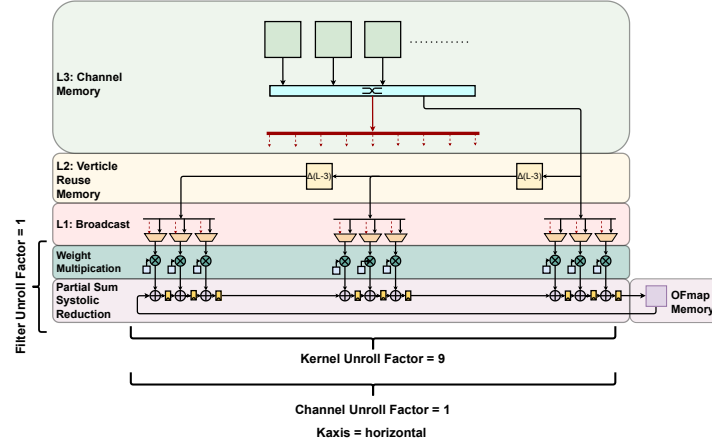
Figure 3.14: Using a systolic reduce and forward to calculate OFmaps

Under this new streaming based interpretation of the accesses in the IFmap memory hierarchy, the delay elements in the systolic reduction scheme in Figure 3.12.b are represented as time shifts in the stream function $F(i, t)$. These time shifts are represented in the new delayed access function $A_\Delta(i, t)$.

$$A_\Delta(i, t) = C_i n^2 + Y_i n + (i - \lfloor \frac{i}{K} \rfloor K) + t - i \tag{3.16}$$

$$A_\Delta(i, t) = \lfloor \frac{\lfloor \frac{i}{K} \rfloor}{K} \rfloor^2 + (\lfloor \frac{i}{K} \rfloor) \bmod K + \underbrace{(-\lfloor \frac{i}{K} \rfloor K)}_{X_i'} + t \tag{3.17}$$

$$\tag{3.18}$$

Substituting the InitialOffset function in A_Δ allows us to simplify the column offset. This yields a new column offset X_i'. The final delayed access function's initial offset becomes insensitive to changes in the port index i that are not multiples of K. This allows us to remove the lowest layer memory along with the systolic array delays in Figure 3.11 and replace both layers with just a series of broadcast buses that span consecutive K groups of IFmap ports provided that we relax the start time constraints to the $\lceil \frac{i}{K} \rceil$ for each group of ports $\lfloor \frac{i}{K} \rfloor$. Delays in accessing IFmap data elements accross K groups of ports as well as accross K^2 groups of ports accessing different channels still remain. This simplifying the hierarchy by removing the systolic delays thus still requiring complex delayed reads from the IFmap hierarchy which necessitates smart SRAMS whose access times can be programmed. A discussion of these smart memories is presented in **??**. The final hardware implementation with the added IFmap memory hierarchy optimization discussed in this section is

given in Figure 3.14. Figure 3.14 shows the broadcast busses for every group of 3 processing engines as well as the 1x1 vertical broadcast busses highlighted in red.

3.3 HERO-T: A Hybrid GEMM and Direct Conv. Accelerator Template

TEMPO's analytical model is hardware implementation agnostic Tempo optimizes utilization given a library of networks + a pe budget TEMPO reports average utilization, latency, and access count statistics Then move on hero-t-sim to cycle accurate simulation results Show performance for some popular networks
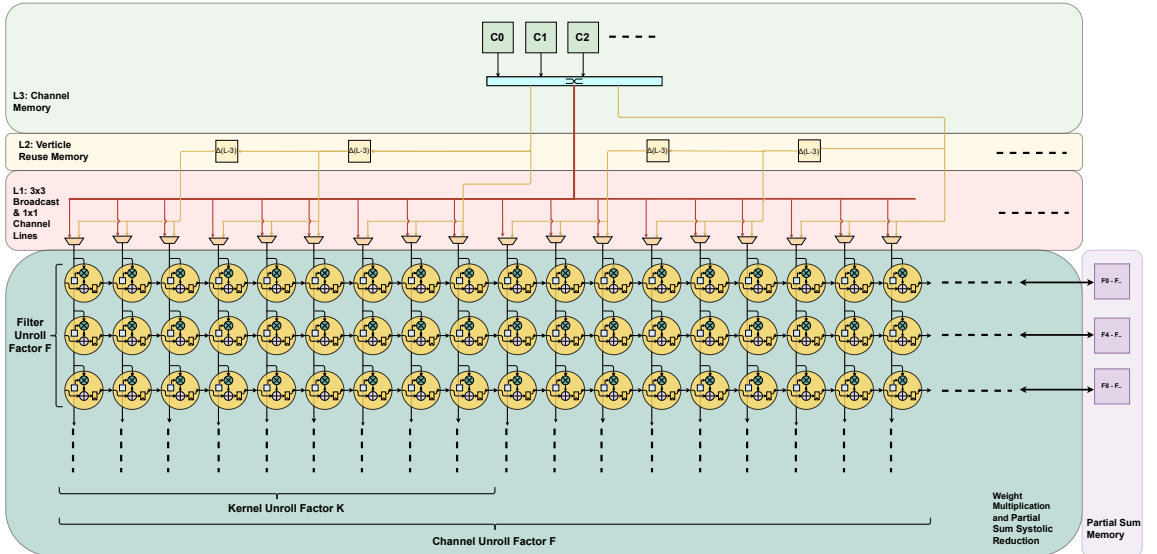
Figure 3.15: Hardware Implementation Taxonomy adapted from [7]
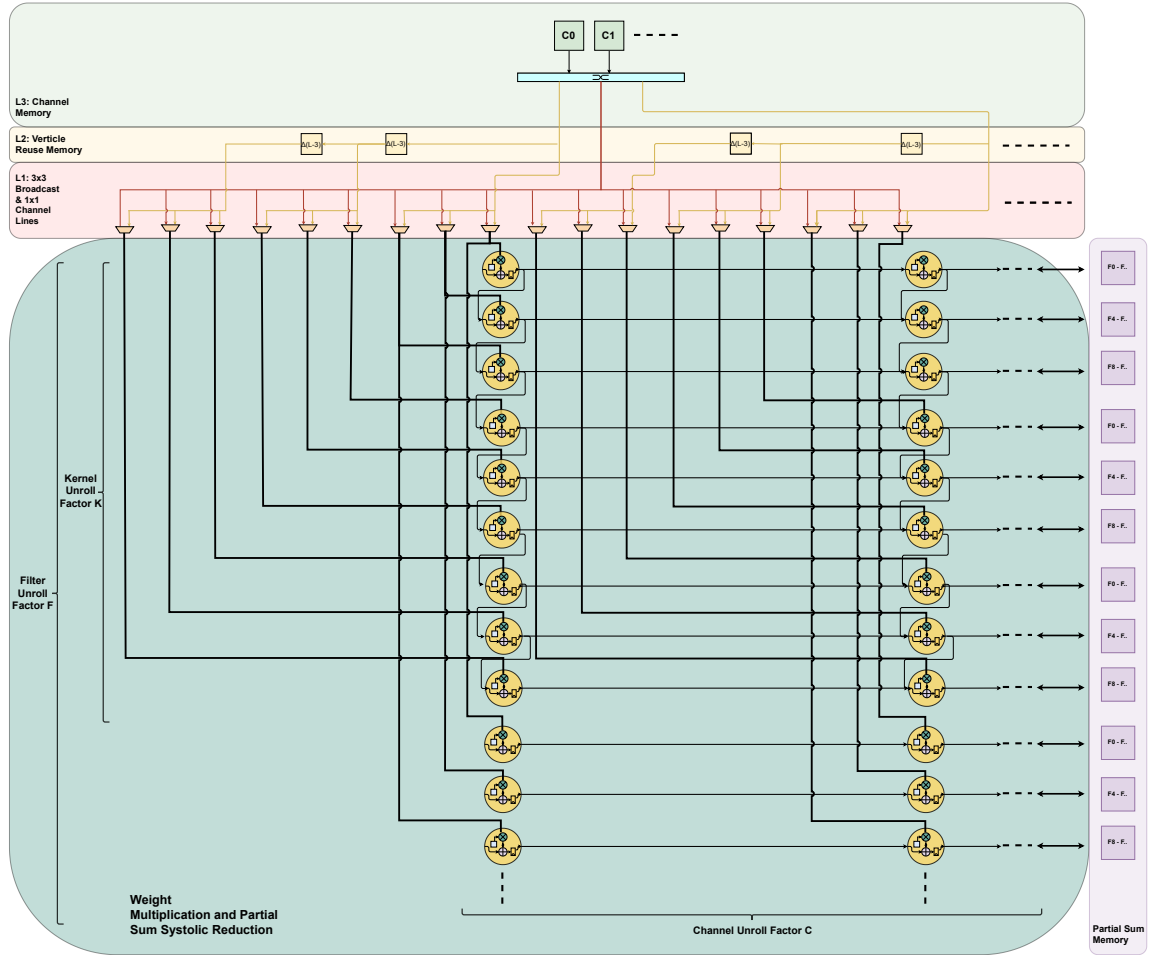
Figure 3.16: Hardware Implementation Taxonomy adapted from [7]

Chapter 4

Architecture Dimensioning

4.1 Layer Equivalence

Accelerator generality can be maintained by supporting general matrix multiplication operations as well as convolution operations common in many modern deep neural networks. Convolution operations can be converted into general matrix multiplication through the use of lowering and lifting techniques like Im2col discussed in [1]. To support matrix multiplication within a convolution accelerator we can reporpose existing compute and memory hardware on chip to perform both GEMM and convolutions operations or we can establish a mathematical equivelence between GEMM operations and Conv by reinterpret GEMM into a special case of convolution, namely convolutions with a 1x1 kernel size. This avoids the overhead of reporposing existing convolution hardware to support GEMM. In subsection 4.1.1, a proof for the equivelence between GEMM and 1x1 Convolutions is given. Additionally, in subsection 4.1.2 the afformentioned proof will be used in tandem with the approach in [1] to provide support for arbitrary convolution operations. Finally in subsection 4.1.3 a discussion of the overheads associated with the approach in subsection 4.1.2 is given.

4.1.1 Functional equivelence between GEMM and 1x1 Convolutions

We can establish functional equivelence between GEMM and 1x1 convolutions with the following proof. An illustration of this proof is given in Figure 4.1. Given two matricies $A \in \mathbb{R}^{Z \times C}$ and $B \in \mathbb{R}^{C \times F}$, let $R \in \mathbb{R}^{Z \times F} = A.B$. A different way to express the matrix multiplication $A.B$ is Equation 4.1.

$$R[z][f] = \sum_{c=0}^{C-1} A[z][c] \times B[c][f]$$
$$\forall z \in [0, n^2 - 1]$$
(4.1)

Transposing A and B yields $\hat{A} \in \mathbb{R}^{C \times Z}$ and $\hat{B} \in \mathbb{R}^{F \times C}$. Using the identity $(A.B)^T = B^T.A^T$ we can rewrite Equation 4.1 as Equation 4.2 where $\hat{R} \in \mathbb{R}^{F \times Z}$

$$\hat{R}[f][z] = \sum_{c=0}^{C-1} \hat{B}[f][c] \times \hat{A}[c][z]$$
$$\forall z \in [0, Z - 1]$$
(4.2)

We can reshape $\hat{A}$ and $\hat{B}$ using Equation 4.3 into 3D tensors by adding an additional dimention of size 1 for $\hat{A}$ and 2 additional dimentions of size 1 for $\hat{B}$.

$$\hat{A} \xrightarrow{Reshape} \hat{A} \in \mathbb{R}^{C \times Z \times 1} \quad \hat{B} \xrightarrow{Reshape} \hat{B} \in \mathbb{R}^{F \times C \times 1 \times 1}$$
(4.3)

Applying Equation 4.3 to Equation 4.2 yields Equation 4.4 where $\hat{R} \in \mathbb{R}^{F \times Z \times 1}$ remains the transposed output of $A.B$.

$$\hat{R}[f][z][0] = \sum_{c=0}^{C-1} \hat{A}[c][z][0] * \hat{B}[f][c][0][0]$$
$$\forall z \in [0, Z - 1]$$
(4.4)

Adding kernel summations to Equation 4.4 yields Equation 4.5 which is equivelent to a 1x1 convolution of stride 1. To recover R from $\hat{R}$ we can reshape $\hat{R}$ by removing the last dimention and then transpose it.

$$\hat{R}[f][z][0] = \sum_{c=0}^{C-1} \sum_{k_x=0}^{1} \sum_{k_y=0}^{1} \hat{A}[c][y + ky][x + kx] * \hat{B}[f][c][k_y][k_x]$$
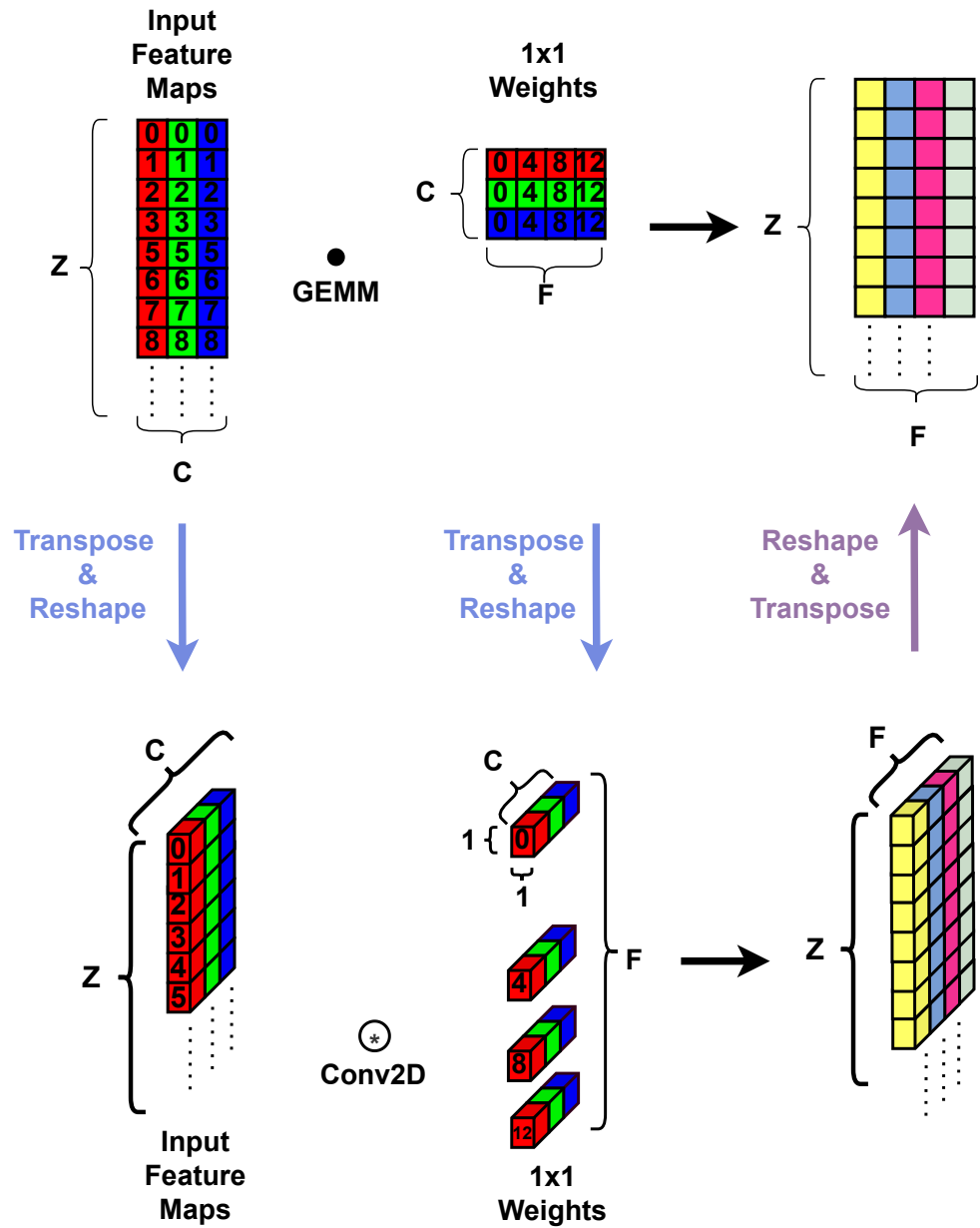$$\forall y \in [0, Z - 1] \wedge x = 0$$
(4.5)

Figure 4.1: GEMM and 1x1 Convolution Equivelence

4.1.2 Supporting unsupported kernel sizes in a direct convolution accelerator

We can support previously unsupported kernel sizes by combining the GEMM to 1x1 Conv conversion in subsection 4.1.1 with any tensor lowering/lifting approach in [1]. Lowering converts a convolution into a GEMM operation, and the approach in subsection 4.1.1 reinterprets that operation as another 1x1 Convolution. This approach allows any convolution accelerator that can support 1x1 convolution operations to support any arbitrary convolution operation. A visual illustration for this technique is presented in Figure 4.2. To demonstrate this approach we begin by lowering both IFmap using Equation 2.3 and Weights using Equation 2.4. This results in two matricies IFmap and Weights in Equation 4.6. Lowering should be performed if the kernel size of the Weight tensor is unsupported $K' \notin \{SupportedKernels\}$.

$$
\begin{aligned}
IFmap \in R^{C \times n \times n} &\xrightarrow{BalancedLowering} I\hat{F}map \in R^{nm \times K'C} \\
Weight \in R^{F \times C \times K' \times K'} &\xrightarrow{BalancedLowering} W\hat{e}ight \in R^{K'C \times K'F}
\end{aligned}
\tag{4.6}
$$

After lowering both tensors, we apply the transformations in Equation 4.7 to reinterpret the anticipated GEMM operation that occurs after lowering into a 1x1 convolution operation. The transformations are composed of a transpose operation followed by a reshape operation that appends additional dimentions of size 1 to both IFmap and Weights. The transformations yields two new tensors $I\hat{F}map$ and $W\hat{e}ight$.

$$
\begin{aligned}
I\hat{F}map^T \in R^{K'C \times nm} &\xrightarrow{Reshape} I\hat{F}map \in R^{K'C \times nm \times 1} \\
W\hat{e}ight^T \in R^{K'F \times K'C} &\xrightarrow{Reshape} Weight \in R^{K'F \times K'C \times 1 \times 1}
\end{aligned}
\tag{4.7}
$$

After performing the transformations in Equation 4.7 the output $O\hat{F}map_{prelift}$ can be calculated after performing a 1x1 convolution in Equation 4.8 using the $I\hat{F}map$ and $W\hat{e}ight$ tensors.

$$
O\hat{F}map_{prelift} \in R^{K'F \times nm \times 1} = I\hat{F}map * W\hat{e}ight
\tag{4.8}
$$

Finally we can lift $O\hat{F}map_{prelift}$ by first reshaping it into a 2D matrix by dropping the last dimension and then transposing it. After that, we can apply balanced lifting in Equation 2.6 to get the final OFmap in Equation 4.9.

$$
\begin{aligned}
O\hat{F}map_{prelift} \in R^{K'F \times nm \times 1} &\xrightarrow{Reshape} OFmap_{prelift} \in R^{K'F \times nm} \\
OFmap_{prelift}^T \in R^{nm \times FK} &\xrightarrow{BalancedLifting} OFmap \in R^{F \times m \times m}
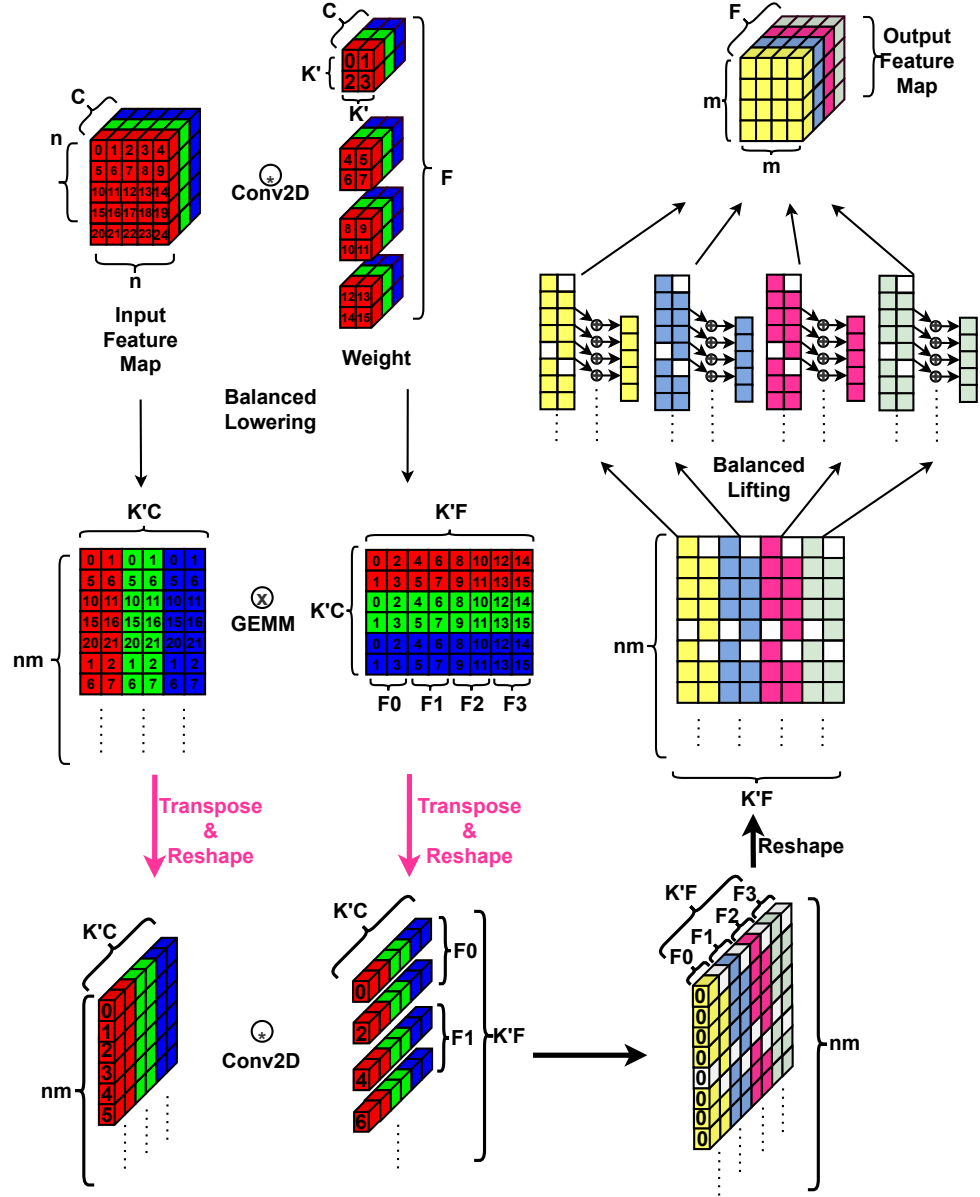\end{aligned}
\tag{4.9}
$$

Figure 4.2: Illustration of approach Conv2Gemm2Conv approach

4.1.3 Overhead of extending support

Lowering and lifting introduce additional overheads with regards to latency and tensor sizing. The latency for performing balanced lowering and lifting is m^2K for a layer with a Weight tensor $\mathbb{R}^{F \times C \times K \times K}$ and an OFmap tensor $\mathbb{R}^{F \times m \times m \times}$. While lowering and lifting can be performed by a convolutions accelerator, in this thesis it is assumed that a software processor on the same chip performs these operations. Lowering also introduces duplicate data elements in the IFmap tensor thus increasing it's overall size. In this thesis, it is assumed that on-chip memory can account for this increase and that any additional DRAM accesses incurred from lowering will be included in energy calculations when reporting energy consumption of the accelerator.

To enable GEMM operations using the approach in subsection 4.1.1 both input and output matricies are transposed and reshaped. All reshape operations discussed in this chapter add a dimention of size 1 to the data and they incur no data reorganization overhead. Additionally, all transpose operations are assumed to be performed during transfer to and from accelerator on-chip and thus incur no latency penalty. A discussion of how transfers to and from on-chip memory can mask the latency of transposing matricies is left as part of future work along with incorporating lowering and lifting into the accelerator.

4.2 Exploring the dataflow design space with TEMPO

From the previous section we have concluded that loops F, C, KY and KX are all unroll targets, and KY and KX loops should be unrolled assuming that 1x1 and 3x3 kernels are supported directly. Additionally, the loop ordering of F and C loops was discussed as well as it's implications with regards to on-chip memory sizing. What remains of the dataflow design space is the unroll factors for F and C loops as well as the accelerator spatial axis mapping for all unrolled loops F, C, KY, KX. From this point these parameters will be referred to as accelerator template paremeters from which a concrete accelerator instance can be defined. These accelerator template parameters define the number of processing engines allocated to process channels, filters, and kernels concurrently in the concrete architectures. An illustration of this PE allocation is present in Figure 4.5. The space of possible unroll factors is as large as the space of possible loop upperbounds for the afformentioned unrolled loops. However, as discussed earlier, some combinations of loop upperbounds are unlikely in real networks. Additionally, spatial axis mapping affects the effective unroll factors when executing different convolution layers than the ones assumed when unrolling said loops. This further
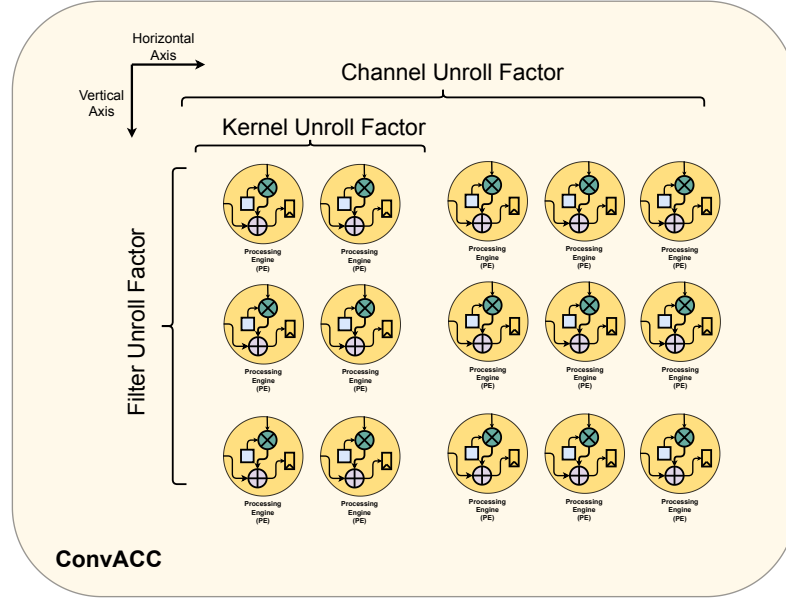
Figure 4.3: GEMM and 1x1 Convolution Equivelence

expands the design space of a concrete accelerator's template parameters. To effectively explore the space of loop unroll factors and accelerator spatial axis mapping we introduce TEMPO, a dataflow exploration and analysis tool used to optimize an accelerator's weight stationary dataflow based on a target CNN library as well as an arbitrary objective function. A discussion of TEMPO's algorithm model is presented in subsection 4.2.1 as well as it's analytical model in in subsection 4.2.2. Additionally, results of running TEMPO on CIGAR's library of CNNs are presented in subsection 4.2.3.

4.2.1 TEMPO Algorithm

TEMPO's algorithm is presented in algorithm 2. TEMPO explores the space of possible filter and channel unroll factors as well as kernel axis mappings by exhaustively iterating through the space of possible values. TEMPO expects the following inputs.

- Processed $model_{dict}^{stats}$ from CIGAR

- An objective function obj_fn

- Maximum pe_{budget}

- Set of kernels supported directly $kernels_{supported}$

49

Tempo then produces an optimal filter, channel unroll factors and kernel axis mapping that maximizes the given objective function under the pe_{budget} constraint specified.

In algorithm 2 TEMPO effectively runs an optimization program that performs the optimization in Equation 4.10 where for some arbitrary objective function obj_fn is evaluated using some template config and the model library. The objective function is a function that evaluates an architectures score based on any of metrics discussed in subsection 4.2.2 and layers in the model library $model_{dict}^{stats}$. Prior to the search being performed algorithm 2 converts all layer not supported directly in the model to 1x1 equivent layers based on the method discussed in chapter 4.

$$\underset{f_{unroll}, c_{unroll}, k_{axis}}{\mathrm{argmax}} \quad obj\_fn(f_{unroll}, c_{unroll}, k_{axis}, ModelLibrary)$$

$$\text{subject to} \qquad\qquad (4.10)$$

$$F_{unroll}.C_{unroll} <= Pe_{budget}$$

Algorithm 2 TEMPO

Input: $model_{dict}^{stats}, obj\_fn, kernels_{supported}, pe_{budget}$

Output: $template_{config}^{opt}$

1: **function** TEMPO_RUN($model_{dict}^{stats}, obj\_fn, kernels_{supported}, pe_{budget}$)
2:      $max_{score} \leftarrow -\inf$
3:      $template_{opt} \leftarrow nil$
4:      $\hat{model}_{dict}^{stats} \leftarrow convert\_all\_unsupported\_layers(model_{dict}^{stats}, kernels_{supported})$
5:      **for** $f_{unroll} \leftarrow factors(pe_{budget})$ **do**
6:          **for** $k_{axis} \leftarrow \{Verticle, Horizontal\}$ **do**
7:              $c_{unroll} \leftarrow \lfloor \frac{pe_{budget}}{f_{unroll}} \rfloor$
8:              $template_{score} \leftarrow obj\_fn(f_{unroll}, c_{unroll}, k_{axis}, \hat{model}_{dict}^{stats})$
9:              **if** $max_{score} < template_{score}$ **then**
10:                  $max_{score} \leftarrow template_{score}$
11:                  $template_{opt} \leftarrow template_{config}$
12:              **end if**
13:          **end for**
14:      **end for**
15:      **return** $template_{config}^{opt}$
16: **end function**

4.2.2 TEMPO analytical model

4.2.2.1 Layer equivelence

In TEMPO's analytical model, an automatic layer conversion step is performed to change the dimensionality of the IFmap and Weight tensors on the basis of whether a layer's kernel size is supported directly or not. This conversion follows the approach outlined in chapter 4 which is used to extend support to unsupported convolution layers. Wheather or not a convolution layer's kernel size is supported directly has an effect on the assumed dimensionalities of the IFmap and Weight tensors as well as the kernel loops unroll factor K. Kernels are assumed to be symmetric so both kernel KY and KX loops and share a single unroll factor K_{unroll}. If the convolution layer's kernel size is supported directly no changes are assumed to have been made to the dimensionality of the input. The kernel unroll factor is then equal to the kernel size of the layer in accordance with the conclusions drawn from subsubsection 3.1.2.2. However, if a convolutions layer's kernel size is not supported directly, the layer's kernel size is converted to 1x1 as seen in Equation 4.11 and lowering is assumed to have been performed on IFmap and Weight tensors in accordance with the approach discussed in chapter 4. For a convolution layer with IFmap dimensionality $R^{C \times n \times n}$, Weight dimensionality $R^{F \times C \times K \times K}$ and OFmap dimensionality $R^{F \times m \times m}$ the layer's new filter count $\hat{F}$, channel count $\hat{C}$, and IFmap channel size $\hat{Z}$ values are reflected in Equation 4.12.

$$K_{unroll} = \begin{cases} K & K \in \{SupportedKernels\} \\ 1 & K \notin \{SupportedKernels\} \end{cases} \tag{4.11}$$

$$\hat{C} = \begin{cases} C & K \in \{SupportedKernels\} \\ CK & K \notin \{SupportedKernels\} \end{cases}$$

$$\hat{F} = \begin{cases} F & K \in \{SupportedKernels\} \\ FK & K \notin \{SupportedKernels\} \end{cases} \tag{4.12}$$

$$\hat{Z} = \begin{cases} m^2 & K \in \{SupportedKernels\} \\ nm & K \notin \{SupportedKernels\} \end{cases}$$

4.2.2.2 Axis mapping

When determining axis mapping, F and C loops are assumed to be bound to an accelerator's verticle and horizontal spatial axis. Utilizing both axis results in better overall on-chip area

utilization assuming conventional 2 dimensional constraints for chip fabrication. Mapping all loops to the same axis can provide the most flexibility with regards to the allocation of PEs as a resource to process different filters, channels and kernels. However, this complicates on chip connectivity and is not considered by TEMPO. KY and KX loops can then be bound to either the horizontal or veticle axis of an accelerator based on the variable K_{axis}. Depending on which axis KY and KX loops are mapped, the effective unroll factors for F and C loops (F_{eff} and C_{eff}) are changed. If the unrolled kernel loops share the same axis as the C loops, the effective C_{unroll} factor for the C loops is then $\lfloor \frac{C_{unroll}}{K_{unroll}} \rfloor$ which means the effective C unroll factor decreases depending on the size of the kernel unroll factor. This decrease in effective unroll factor arises from the fact that, within the same axis as the C loops, PEs are allocated to process a single K^2_{unroll} kernel. This results in a decrease of PEs available to process other channels concurrently. The same logic applies to F loops if the Kernel loops are mapped to the same axis verticle axis as they are. This idea is presented in Equation 4.13 and Equation 4.14. In both equations F_{unroll} and C_{unroll} are the unroll factors for F and C loops assuming $KY = KX = K = 1$.

$$
C_{eff} = \begin{cases} \lfloor \frac{C_{unroll}}{K^2_{unroll}} \rfloor & K_{axis} = horizontal \\ C_{unroll} & K_{axis} = Verticle \end{cases} \tag{4.13}
$$

$$
F_{eff} = \begin{cases} \lfloor \frac{F_{unroll}}{K^2_{unroll}} \rfloor & K_{axis} = Verticle \\ F_{unroll} & K_{axis} = Horizontal \end{cases} \tag{4.14}
$$

4.2.2.3 Metric: Utilization

TEMPO models accelerator utilization based on how the template parameters (loop unroll factors and loop axis mapping) tile and pad a convolution layer's stationary weight tensor. Kernel axis mapping is assumed to be inflexible across accelerator spatial axis at runtime. An illustration of TEMPO's utilization model in action is present in Figure 4.4. In Figure 4.4 a layer with a weight tensor of dimensionality $R^{6 \times 3 \times 2 \times 2}$ is tiled and padded based on the template parameters $C_{unroll} = 8$, $F_{unroll} = 4$, $K_{unroll} = 2$ and axis mapping $K_{axis} = horizontal$. Based on these template parameters the effective filter and channel unroll factors are $F_{eff} = 4$, $C_{eff} = 2$. These unroll factors create $\lceil \frac{\hat{C}}{C_{eff}} \rceil = 2$ horizontal tiles and $\lceil \frac{\hat{F}}{F_{eff}} \rceil = 2$ verticle tiles assuming padding has been applied. The weight tensor in Figure 4.4 is then reshaped into a 2D matrix of dimensionality $R^{8 \times 16}$ with additional padding. The total number of tiles is then reflected in Equation 4.15.
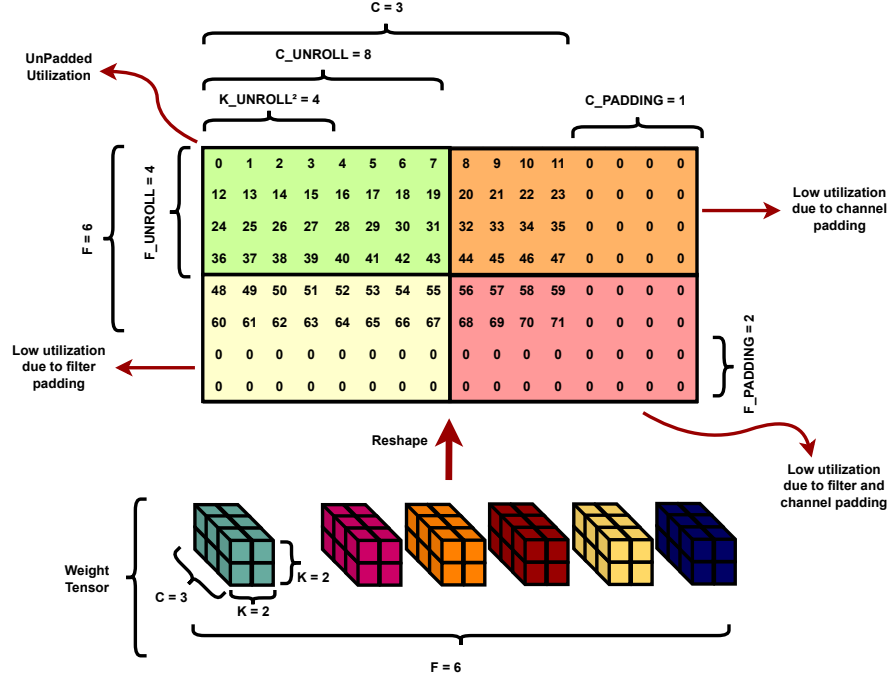
Figure 4.4: GEMM and 1x1 asd Equivelence

$$Count_{Tiles} = \lceil \frac{\hat{F}}{F_{eff}} \rceil \lceil \frac{\hat{C}}{C_{eff}} \rceil \tag{4.15}$$

Utilization is calculated on a per-tile basis. There are two different types of tiles, padded and unpadded, each with their own utilization calculation. Layer utilization is then an average of the utilizations of each tile type weighted by their frequency of occurence in the layer as reflect in Equation 4.16. For brevity each of the utilization equations are multiplied by their frequency of occurence in the same equation.

$$LayerUtilization = \frac{utilization_{Tiles}^{UnPadded} + utilization_{Tile(s)}^{Padded}}{Count_{Tiles}} \tag{4.16}$$

The first tile type is the unpadded tile illustrated in Figure 4.4 as the green tile. Utilization is calculated using Equation 4.17. In this tile utilization is assumed to be 1 and it's frequency of occurence depends on the number of unpadded tiles in the layer $\lfloor \frac{\hat{F}}{F_{eff}} \rfloor \lfloor \frac{\hat{C}}{C_{eff}} \rfloor$.

$$utilization_{Tiles}^{UnPadded} = 1.\lfloor \frac{\hat{F}}{F_{eff}} \rfloor \lfloor \frac{\hat{C}}{C_{eff}} \rfloor \tag{4.17}$$

The second tile type is the padded tile of which there are three variations depending on the reason for padding the tile. The utilization for all padded tiles weighted by their frequencies of occurence is given in Equation 4.18.

$$
\begin{aligned}
utilization_{Tile(s)}^{Padded} = \ &utilization_{ChannelTiles}^{Padded} \\
&+ utilization_{FilterTiles}^{Padded} \\
&+ utilization_{ChannelAndFilterTiles}^{Padded}
\end{aligned}
\tag{4.18}
$$

If the allocation of PEs for channel loops exceeds avaliable channels to be processed in the tile, then that tile will be padded. The padding in that tile results in reduced PE utilization. An illustration of that padded tile variation is present in Figure 4.4 as the orange tile. The calculation for the weighted utilization in that tile variation is given in equation Equation 4.19. To determine if a a padded channel exists or not we can check if $\hat{C} \bmod C_{eff} > 0$ is true. If that condition is true, padded channel tiles exist in the layer and their weighted $utilization_{ChannelTiles}^{Padded}$ is then a function of how many PEs are active in the tile $\frac{(\hat{C} \bmod C_{eff})F_{eff}K_{unroll}^2}{Count_{pe}}$ multiplied by the frequency of occurence. $\lfloor \frac{\hat{F}}{F_{eff}} \rfloor$. If $\hat{C} \bmod C_{eff} = 0$ then there are no padded channel tiles so $utilization_{ChannelTiles}^{Padded} = 0$.

$$
utilization_{ChannelTiles}^{Padded} =
\begin{cases}
\frac{(\hat{C} \bmod C_{eff})F_{eff}K_{unroll}^2}{Count_{pe}} \cdot \lfloor \frac{\hat{F}}{F_{eff}} \rfloor & \hat{C} \bmod C_{eff} > 0 \\
0 & \hat{C} \bmod C_{eff} = 0
\end{cases}
\tag{4.19}
$$

If the allocation of PEs for filter loops exceeds avaliable filters to be processed in the tile, then that tile will be padded. This another variation of a padded tile and the weighted utilization for that tile variation is calculated using Equation 4.20 and is illustrated in Figure 4.4 as the yellow tile.

$$
utilization_{FilterTiles}^{Padded} =
\begin{cases}
\frac{C_{eff}(\hat{F} \bmod F_{eff})K_{unroll}^2}{Count_{pe}} \cdot \lfloor \frac{\hat{C}}{C_{eff}} \rfloor & \hat{F} \bmod F_{eff} > 0 \\
0 & \hat{F} \bmod F_{eff} = 0
\end{cases}
\tag{4.20}
$$

Finally the last padded tile variation is the tile padded due to the excess allocated of PEs for both filter and channel loops. This type of tile is illustrated in Figure 4.4 as the red tile. To determine if a tile like this exists we can evaluate the condition $\hat{F} \bmod F_{eff} > 0 \wedge \hat{C} \bmod C_{eff} > 0$ is true. If it there exists exactly one tile where utilization is reduced due to excess allocation of PEs for filter and channel loops. The equation to calculate weighted utilization in this padded tile variation is given in Equation 4.21.

$$utilization_{Channel\&FilterTile}^{Padded} = \begin{cases} \frac{(\hat{C} \bmod C_{eff})(\hat{F} \bmod F_{eff})K_{unroll}^2}{Count_{pe}} & \hat{F} \bmod F_{eff} > 0 \wedge \hat{C} \bmod C_{eff} > 0 \\ 0 & else \end{cases}$$

$$(4.21)$$

4.2.2.4 Metric: Latency

Estimating latency follows the same tiling model discussed the previous subsection. The latency of executing a layer based on the template paremeters chosen is given in Equation 4.22. Latency is a function of the number of tiles present in the layer multiplied by the number of cycles spent processing a single IFmap channel $\hat{Z}$ plus the additional latency incured due to lowering lifting depending on the support for the layer's kernel size. Latency for lowering and lifting is given in Equation 4.23. If the kernel is supported directly, no additional lowering and lifting penalties are incurred, otherwise penalties are calculated based on the number of operations necssary to lower the IFmap and Weight tensors plus the number of operations to lift the OFmap. Lowering and lifting are assumed to be performed by a software based co-processor. The latencies associated with lowering and lifting can be eliminated if these operations are incoporated into the processor however, that is left as part of future work.

$$Latency = \hat{Z}.Count_{Tiles} + Latency_{Lowering} + Latency_{Lifting} \qquad (4.22)$$

$$Latency_{Lowering} = Latency_{Lifting} = \begin{cases} 0 & K \in \{SupportedKernels\} \\ m^2K & K \notin \{SupportedKernels\} \end{cases} \qquad (4.23)$$

4.2.2.5 Metric: Memory access counts

Following the tiling model discussed earlier, memory access counts are calculated based on how the template paremeters tile the layer's weight tensor. Access counts for IFmaps are given in Equation 4.24, OFmap access counts are giving in Equation 4.25 and finally weight access counts are given in Equation 4.26.

$$IFmap^{AccessCount} = ((\hat{Z}K_{unroll}^2)(\lfloor\frac{\hat{C}}{C_{eff}}\rfloor C_{eff} + \hat{C} \bmod C_{eff}))\lceil\frac{\hat{F}}{F_{eff}}\rceil \qquad (4.24)$$

$$OFmap^{AccessCount} = 2 * \hat{Z}(\lfloor\frac{\hat{F}}{F_{eff}}\rfloor F_{eff} + \hat{F} \bmod F_{eff})\lceil\frac{\hat{C}}{C_{eff}}\rceil \qquad (4.25)$$
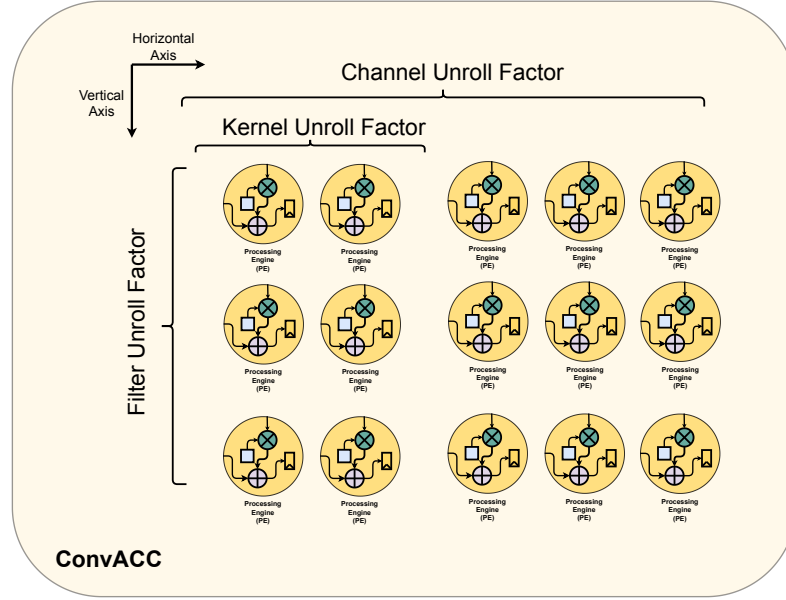
Figure 4.5: GEMM and 1x1 Convolution Equivelence

$$
\begin{aligned}
Weight^{AccessCount} = {} & \hat{Z}((C_{unroll}F_{unroll})(\lfloor\frac{\hat{C}}{C_{eff}}\rfloor\lfloor\frac{\hat{F}}{F_{Feff}}\rfloor) \\
& + (C_{unroll}F_{eff})(\lfloor\frac{\hat{C}}{C_{eff}}\rfloor\hat{F} \bmod F_{eff}) \\
& + (C_{eff}F_{unroll})(\lfloor\frac{\hat{F}}{F_{eff}}\rfloor\hat{C} \bmod C_{eff}) \\
& + (C_{eff}F_{eff})(\hat{F} \bmod F_{eff} * \hat{C} \bmod C_{eff}))
\end{aligned}
\tag{4.26}
$$

4.2.3 TEMPO results

4.2.3.1 Assumed objective function

Since TEMPO expects an objective function to maximize based on any or a combination of all the discussed metrics in subsection 4.2.2 Equation 4.27 defines an objective function based solely on the average layer utilization metric over the entire set of convolution layers in CIGAR's model library. Layer utilization is evaluated based on the discussion in subsubsection 4.2.2.3.

$$
obj\_fn \leftarrow average(\{LayerUtilization(layers)|\forall layers \in m, \forall m \in \{ModelLibrary\}\})
\tag{4.27}
$$

Chapter 5

On-Chip Data Orchestration

To coordinate IFmap reads, OFmap read-modify-writes and Weight reads based on the final implementation in section 3.2 we need smart programmable memories that can 1) perform timed reads and writes between themselves and processing engines and 2) perform timed data transfers between themselves and other programmable memories. In this chapter, we introduce SAMs, a programmable memory primitive that can execute descriptor based programs. Depending on the composition of these descriptor based programs, timed reads and writes can be made by on SAMs to and from processing engines. Additionally, with sufficient connectivity between SAMs as well as implicit coordination between different SAM programs we can orchestrate timed data transfers between SAMS. In this chapter we first discuss the structure of a SAM in section 5.1 followed by the functional behavior of a SAMs address generator controller in section 5.2. We then introduce descriptor based programs in section 5.3, specifically the different types of descriptors available in subsection 5.3.1 as well as the different types of memory transactions possible using coordinating descriptor based programs in subsection 5.3.2. Finally, in section 6.2 we show how SAMs can be used to schedule convolution operations in the final hardware implementation of section 3.2.
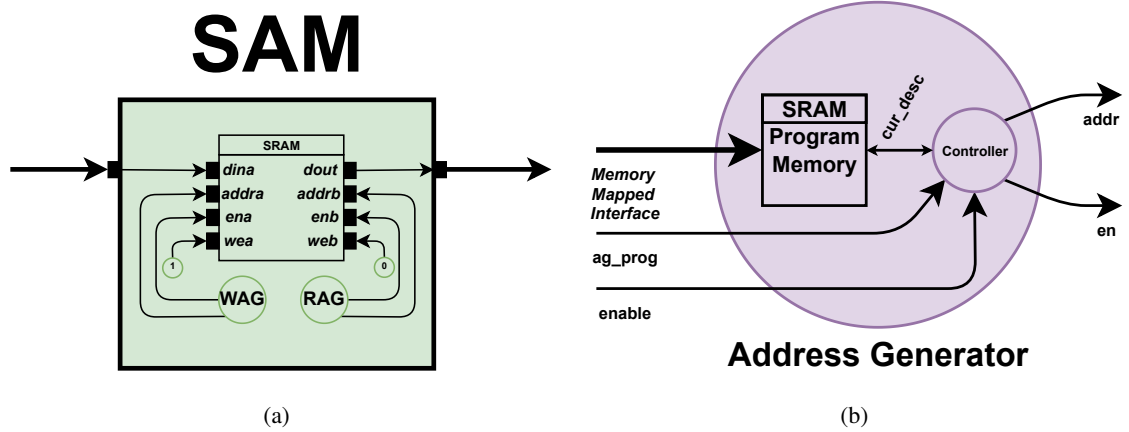
Figure 5.1: Illustration of different dataflow implementations adapted from [14] (a) blah (b) blah (c) blah (d) blah

5.1 Structure of a SAM

In Figure 5.1.a SAMS are composed of an address generator and a data sram. Address generators are attached to ports of an SRAM. They control the address and enable ports for each SRAM port. The port behavior (read or write) is set by a memory mapped register attached to the write enable pins of each port. Address generators are programmable modules within SAMs that generate address streams based on descriptor programs. These address streams are then fed to the SAMs data SRAM. In Figure 5.1.b, address generators are composed of a controller attached to a program memory SRAM. Depending on the sizing requirements of the descriptor programs, program memory SRAMs can be replaced with register files containing all relevant descriptors. SAM address generators are equipped with an external memory mapped interface to allow transfer of descriptor programs from an a software based co-processor.

5.2 Address generator controller

The finite state machine of address generator controllers is presented in Figure 5.2. After an initial reset, the controller waits until the ag_prog signal is asserted thus indicating that the generator is in the program state and is awaiting to receive a descriptor based program from the external memory mapped interface. Once the program is confirmed to be have been written by the external interface the ag_prog signal can be de-asserted followed by the assertion of the enable signal. When that occurs the controller transitions into the execute state in which it loads the first descriptor
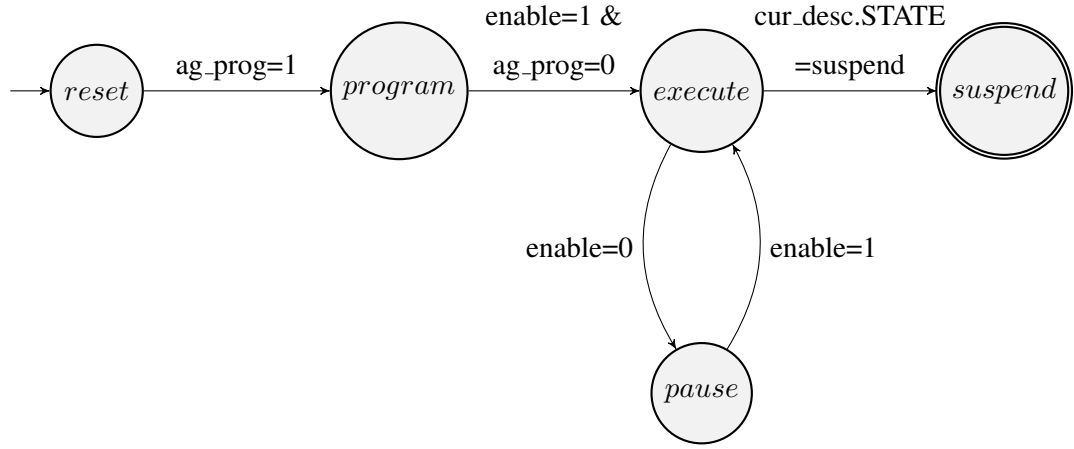
Figure 5.2: Address generator Finite State Machine

and executes it. If the enable signal is de-asserted for any reason the controller enters a pause state. When the enable signal is re-asserted the controller goes back to the execute state. Once a descriptor is retired, the controller reads the next descriptor from the program memory and begins executing it without leaving the execute state. If the controller's cur_desc pointer points to a suspend descriptor execution terminates the controller enters a suspend state.

5.3 Descriptor based programs

Descriptor based programs are inspired by [6] where the authors illustrates different ways to program a model Blackfin processor's DMA using various descriptor configurations. The main difference between this work's approach to descriptors and [6] is the inclusion of timing and hybrid access/timing descriptors that allow more complicated memory transactions to occur between SAMs.

5.3.1 Descriptor Types

Before discussing descriptor based programs we must first discuss the properties of individual descriptors. Each descriptor can be represented as a struct as depicted in Listing 5.1. In a single descriptor, the state field describes the type of the descriptor. There are four different types of descriptors. Generate descriptors used for generating address streams. Stuttering descriptors used for generating stuttered address streams where the address streams are interrupted at predefined

intervals. Wait descriptors that pause execution of descriptor based programs for a set number of cycles. Lastly, suspend descriptors used to mark the termination of a descriptor based program.

Listing 5.1: Descriptor Struct

```
1  struct Descriptor
2  {
3      DescriptorState state;
4      unsigned int start;
5      unsigned int x_count;
6      int x_modify;
7      unsigned int y_count;
8      int y_modify;
9  };
```

Each descriptor can be thought of as a self contained program. For generate descriptors a C code representation for their execution behavior when they are executed by an address generator is given in Listing 5.3. The output signals from the address generator "en" and "addr" are referred to as global variables in Listing 5.3. Suspend descriptors are the simplest of the different descriptor types. All fields except the state field are set to 0 in the descriptor struct. The state field is set to some predetermined value that represents the SUSPEND state. The next simplest descriptor is the wait descriptor which can be represented using the for loop representation in Listing 5.2 where the SRAM port enable pin is de-asserted and a busy loop runs for x_count cycles. The wait descriptor is used to synchronize different descriptor programs across SAMs as well as create timed writes and reads to and from SAMs.

Listing 5.2: Descriptor as a set of loops

```
1      en = 0;
2      for(int x = 0; x < x_count; x++);
```

Generate descriptors use the y_count, and x_count fields in the descriptor struct to define the upper bounds for two nested loops within which an addr variable is incremented by x_modify in the inner loop and y_modify in the outer loop. The "addr" output signal is initialized with the contents of the start field and the "en" signal is asserted for the duration of the descriptors execution.

Listing 5.3: Descriptor as a set of loops

```
1  en = 1;
2  addr = start;
```

60

```
3   for(int y = 0; y < y_count; y++)
4       for(int x = 0; x < x_count; x++)
5           addr += x_modify;
6       addr += y_modify;
```

For stuttering descriptors, again a C code representation is given in Listing 5.4. As in the previous listing "addr" is initialized with the value in the start field. However, unlike the previous listing the loop structure of the descriptor is different. In Listing 5.4 the outermost loop represents is bounded by the y_count field in the descriptor strut. Within the outer loop two loops exist, one loop dedicated to generating the address stream based on the fields x_count and x_modify while the other is dedicated to pausing for a predetermined number of cycles based on the contents of y_modify field. In between the nested loops the "en" is de-asserted to disable reads/writes to the data SRAM connected to the address generator controller.

Listing 5.4: Descriptor as a set of loops

```
1   addr = start;
2   for(int y = 0; y < y\_count; y++)
3       en = 1;
4       for(int x = 0; x < x_count; x++)
5           addr += x_modify;
6       en = 0;
7       for(int w = 0; w < y_modify; w++);
```

5.3.2 Creating timed memory operations with descriptor programs

Depending on the composition of different descriptor programs one can create timed memory operations with SAMs. An illustration of some of the possible timed operations involving single address generators is given in Figure 5.3. In Figure 5.3.a the contents of C0 are read in a loop. This is achieved by setting the y_modify variable to -X to reset "addr" to the start idx 0. In Figure 5.3.b a wait descriptor is inserted prior to the loop descriptor to introduce a delay in the start time of the loop descriptor.

More complicated memory operations can be performed via the implicit coordination of multiple address generators across SAMs or within the same SAM. An illustration of that coordination is presented in Figure 5.4. In Figure 5.4.a a data transfer between two SAMs is achieved using one read address generator in C0 and one write address generator in C1 as well a connection between the dout pins of C0 and dout pins of C1. The read address generator executes a generate
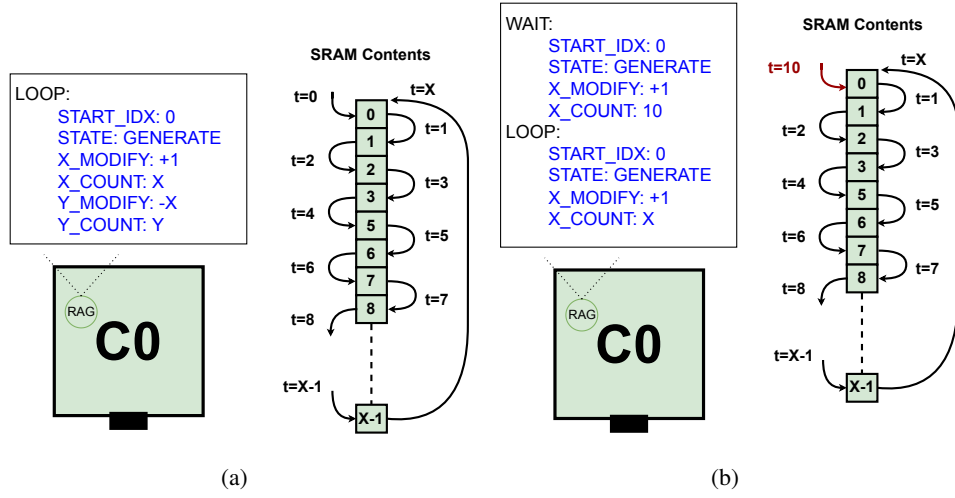
Figure 5.3: Illustration of different dataflow implementations adapted from [14] (a) blah (b) blah (c) blah (d) blah

descriptor that reads out the contents of the SAM. The write address generator waits for 1 cycle then executes a write operation to store the contents of the C0 in C1. These two descriptor programs across two SAMs implicitly coordinate with the inclusion of that wait descriptor. They are each unaware of the program executed by the other. Similarly this implicit coordination can occur between address generators in the same SAM. In Figure 5.4.b a read and a write address generator coordinate to creates a shift register that reads out data received by the SAM after a delay Δ_i. This delay is introduced using similar descriptor programs as in Figure 5.4.a. In Figure 5.4.b the read address generator waits for Δ_i cycles before starting to read the contents written by the write address generator.
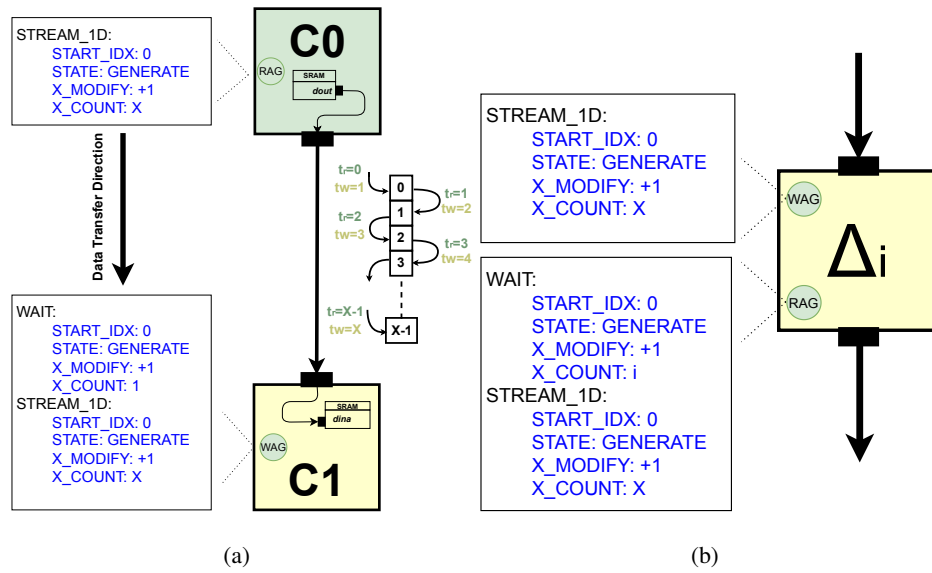
Figure 5.4: Illustration of different dataflow implementations adapted from [14] (a) blah (b) blah (c) blah (d) blah

Chapter 6

Network Compilation

6.1 Layer Decomposition

6.2 Descriptor Generation

We can generate descriptor programs for the memories (now referred to as SAMs) in the final architecture template discussed in section 3.2. These descriptor programs will be used to perform memory operations necessary for the convolution operation to take place in the final architectural template. Since we have two operational modes based on the discussion in chapter 3 1x1/GEMM and 3x3 convolutions we will discuss the descriptor programs required for both of these modes to take place independently of the other. In both modes we will first highlight the memories participating in the operation followed by the required descriptor programs for each of those memories. Please note that muxing plays a part in coordinate the transfer of data between different memories. The programming of muxes in tandem with SAMs is left as part of future work. Additionally, all interactions between SAMs and DRAM are left as part of future work. IFmap and OFmap data is assumed to be read from and written to DRAM before and after the operation of the SAM programs discussed in thi section. Latencies and energy penalties associated with DRAM will be considered in chapter 7 but SAM program generation discussed here is DRAM agnostic.

6.2.1 1x1 convolution programs

To illustrate how SAMs can be programmed to perform a 1x1 convolution we will use the final architecture in section 3.2 and a 1x1 convolution layer with 16 channels and 8 filters as a

driving example. In section 3.2 there are a total of 9 processing engines with all 9 mapped to the accelerator horizontal spatial axis which enables creates an effective an unroll factor of 9 at kernel sizes 1x1. Based on the tiling discussion in subsubsection 3.1.2.2, the architecture tiles the weight tensor into 16 tiles (padding included) as illustrated in Figure 6.1.
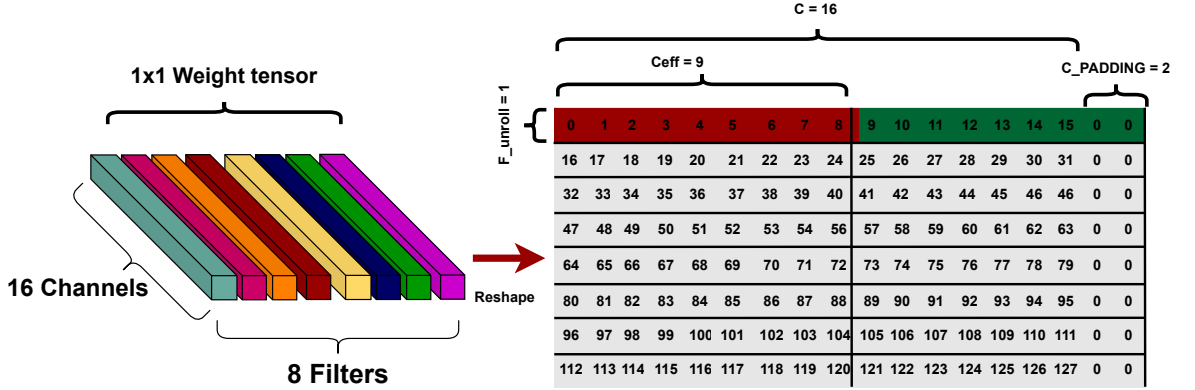

Figure 6.1: Hardware Implementation Taxonomy adapted from [7]

For each weight in the tiles of Figure 6.1 the channel feature map corresponding to that weight has to be streamed into the PE processing the output of that weight. For example, tile highlighted in red needs channels C0-C8 streamed into the PEs storing those for processing. After the red tile is processed, the green tile is loaded into the PEs weight buffer (assuming ASAP scheduling as seen in subsubsection 3.1.2.3). Channels C9-C15 then needs to be streamed into the PEs holding the weights corresponding to those channels. This means that channel memories may need to hold multiple channels that are streamed out depending on the index of the tile being processed. An illustration of how channel feature maps are stored on the channel SAMs is present in Figure 6.2. PEs holding 0 valued weights due to padding have no corresponding channel data so nothing is streamed into them as reflected in the 0 padding of the last channel SAM attached to the 9th PE in Figure 6.2. Additionally, they are assumed to just forward any partial sums/ output feature maps recieved from their input to their output with no modifications.

Since 1x1 convolutions involve entire channel feature maps streamed into PEs with no reuse within a feature map occuring as in the 3x3 case, the only memories that need to be programmed are the L3 channel memories and the OFmap memories. An illustration of the required descriptor programs for the afformentioned memories is given in Figure 6.3. In Figure 6.3 irrelevant
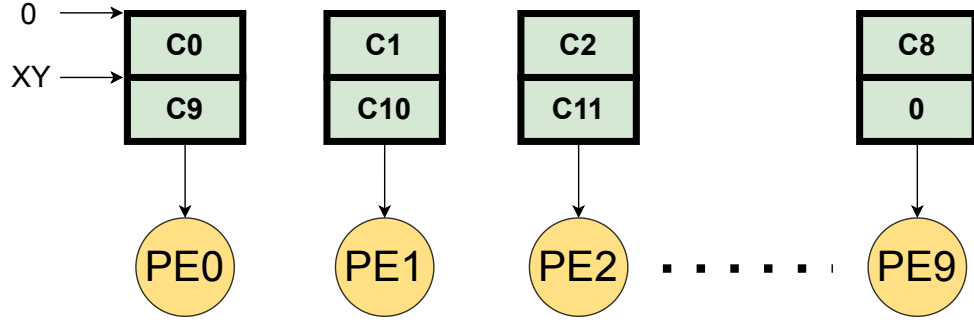
Figure 6.2: Hardware Implementation Taxonomy adapted from [7]

layers and muxing as well as some PEs have been ommited to for brevity.

In Figure 6.3 channel memories can be implemented with SAMs. For each channel SAM there are two descriptors types that appear frequently in their programs, a wait descriptor and generate descriptor. Channel SAMs need to perform timed reads due to the systolic delays arising from the systolic reduction of partial sums into output feature maps. Therefore, an initial wait instruction due to the systolic delay required by each SAM is inserted at the begining of their descriptor programs. The delay defined by the wait descriptor for each SAM depends on the index of the PE that the SAM is connected to. So the first PE's corresponding SAM has no read delay so the x_count variable in the wait descriptor is set to 0. The next PE's channel SAM has a delay of 1 so it's initial weight descriptor's x_count is set to 1. After the initial wait descriptor, each channel SAM needs to stream out a feature map. Depending on the index of the tile being processed, each SAM streams out a different IFmap. What distinguishes each IFmap stored on a channel SAM from another is it's start index. For example, for the first tile highlighted in red, the first PE streams out the IFmap begining at start index 0 with a generate descriptor. The size of that IFmap is assumed to by XY where X and Y are the width and height of the IFmap. The generate descriptor increments the internal address "addr" XY times with "addr" starting at 0. The corresponding generate descriptor that manipulates the "addr" like that is a generate descriptor with an x_count of XY and a start index of 0. When the first PE begins processing the second tile, it reads out the IFmap stored at index XY or more generally $MOD(tile_{idx}, 2).XY$ since each filter has 2 tiles. This generate descriptor is repeated for each tile in the weight tensor assuming that no padding. If a PE is storing a 0 valued weight due to padding the generate descriptor is replaced with a wait descriptor with an x_count of XY. Optimizating descriptors to reduce code size is left as part of future work.

For the OFmap SAM two address generators are required due to the read modify write
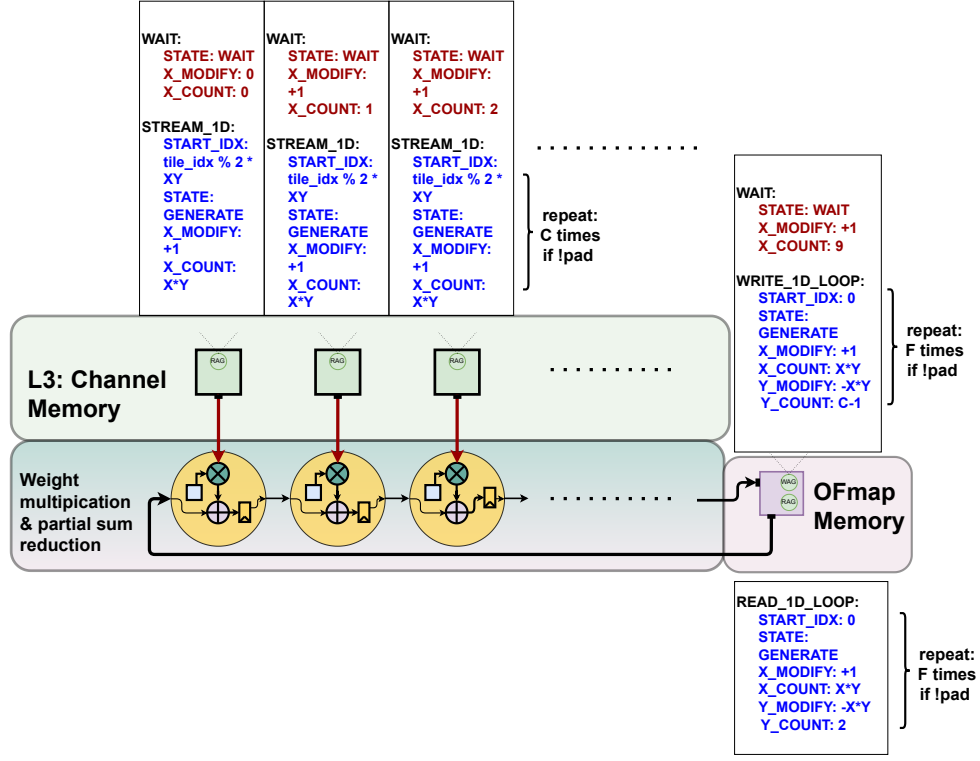
Figure 6.3: Hardware Implementation Taxonomy adapted from [7]

nature of OFmaps. The read port begins reading the layer bias immediately and streams it into the first PE as part of partial sum reduction. All later reads from the OFmap SAM are for partial sums that have yet to be accumulated into OFmaps. The read descriptor required for streaming in bias/partial sums is a generate descriptor that streams out the contents of OFmap in a loop. It achieves this by setting x_count to XY to stream out partial sums of size XY and y_count to 2 which the number of tiles in a filter. To reset the "addr" index of the read descriptor the y_modify is set to $-XY$. This generate descriptor is repeated 8 times where 8 is the number of filters present processed by the PEs assuming no filter padding. Assuming ASAP scheduling as discussed in subsubsection 3.1.2.2 OFmaps are written to DRAM as soon as they are completed and are not kept on chip.

The write port waits for C_{UNROLL} number of cycles to write the first partial sums that will eventually become OFmaps once the filter being processed concludes. IFmaps of XY size less than 9 (the number of PEs in the horizontal axis) will cause additional delay cycles to be introduced via wait descriptors to allow partial sums to propogate through the PEs to reach the OFmap. The reduction performed by the PEs are sequential and not combinatorial, hence the inclusion of reg-

isters between each PE. Alleviating dead cycles due to smaller input feature maps is left as part of future work. The descriptor required for the write address generator are similair to the the read ones with the exception of an additional wait descriptor that gives the first partial sum/ Ofmap time to propogate through the systolic reduction. The delay required by the wait descriptor is equal to the number of PEs present in the horizontal axis. After the wait descriptor comes a generate descriptor that writes the partial sum output/ OFmap output into the OFmap SAM in a loop. The write generatord descriptor is repeated 8 times as well assuming no padding similair to the read generate descriptor loop.

6.2.2   3x3 convolution programs

Chapter 7

HERO Architecture Simulation

so lets say we have a concrete instance of hero-t and we want to assess its performance in a cycle accurate simulator with real layers from a network. We do this with a platform simulator that has a front end that takes a mode library and produces latency, utilization and access cost results.

7.1   Simulation platform

Sim runs a CIGAR pass over the input model library if stats dict not available. It then performs a layer equivelence pass that converts an unsupported convolution layer to an equivelent GEMM using balanced lowering. Overhead Of lowering and lifting is automatically added to the overall latency of the cycle accurate simulation. Simulation only targets conv layers.

7.2   SystemC Model

SystemC models takes in arch config. Arch config usually comes out of a tempo. Currently systemc model only considers horizontal mapping of kernel loops. All muxing/ interconnect logic handled with how individual banks are accessed in the architecture simulation loops. After systemc backend recieves sim config. It instantiates an arch with the required config. It generates an equivelent layer following dimensions of layer sent in from front end and then it generates the descriptor program based on the method discussed in (REFERENCE SAM SUBSECTION) Finally the backend performs a cycle accurate simulation of the instantiated architecture. After simulation concludes, ofmap memory contents are scanned to validate output and if output is valid, latency, access counts and utilization statistics are returned to the platform frontend for high level analysis.
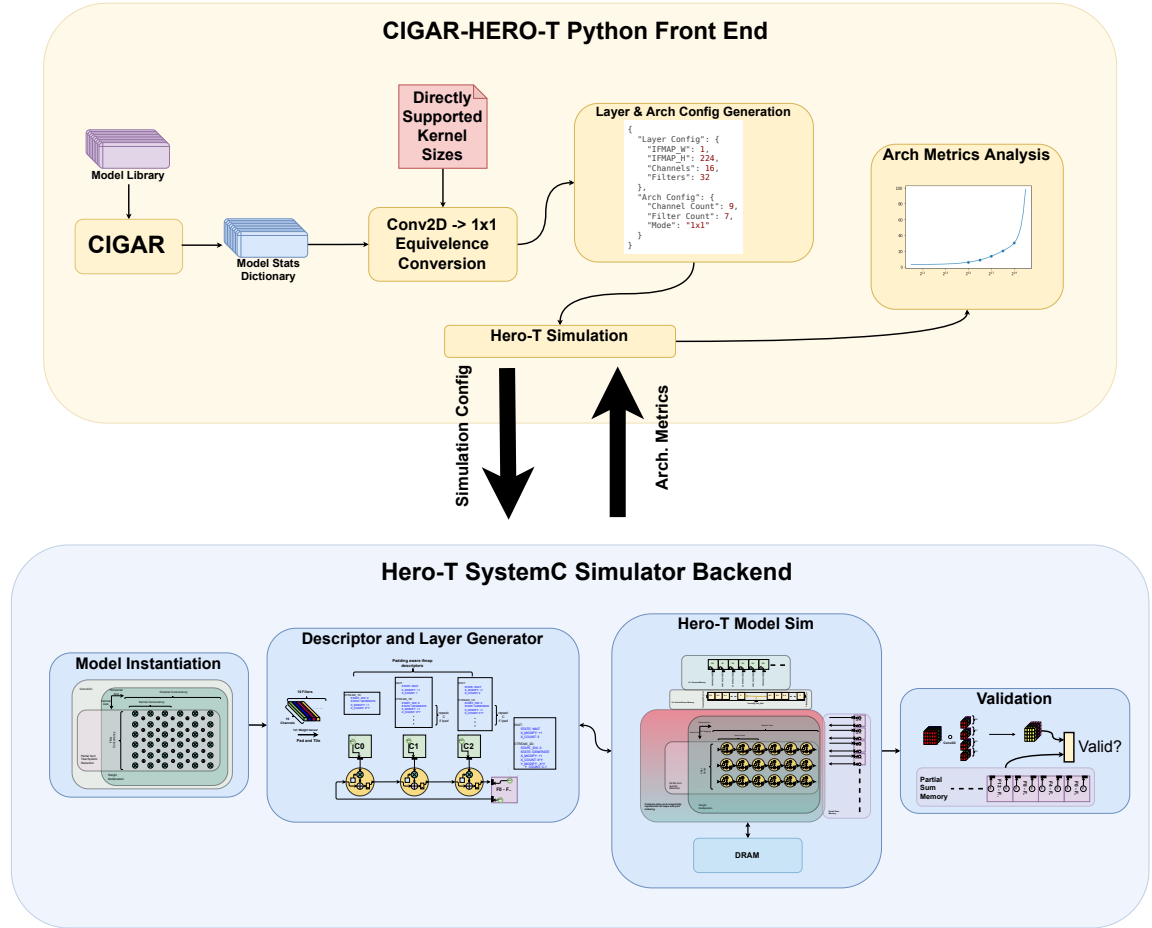
Figure 7.1: Hardware Implementation Taxonomy adapted from [7]

Model is simulated in isolation. DRAM access counts are estimated in the backend but no actual simulation of DRAM occurs.

7.3 Experimental Results

Prominent model's convolution layers were are assessed using the simulation platform namely resnet-50 mobilenetv3 and vgg16. Performance for each of the three conrete architectures suggested by tempo is reported below.
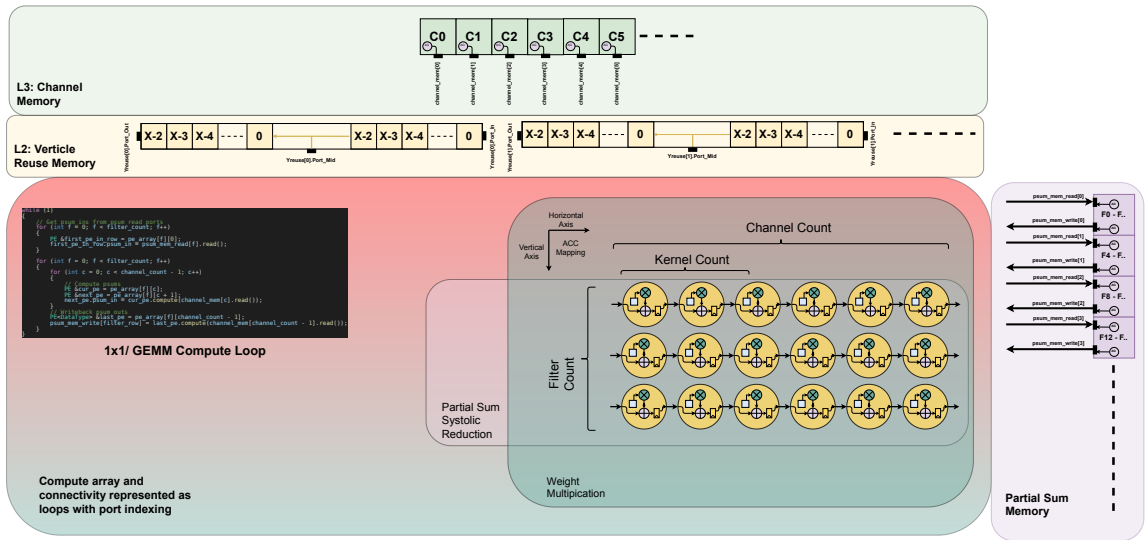
Figure 7.2: Hardware Implementation Taxonomy adapted from [7]

Chapter 8

Related work

8.1 Convolution accelerator architectures

DNN accelerator generator GEMMINI doesn't optimize for direct convolutions

GEMM Based

TPU

Direct

Reduction tree based

Maeri

Systolic array based

Eyeriss

8.2 Convolution accelerator generation techniques

ASIC Based generators

King Kong

Horowitz

Reduction tree based

Maeri

Chapter 9

Conclusion

Writing a long manuscript is easy ... only if one starts early enough.

Bibliography

[1] Firas Abuzaid, Stefan Hadjis, Ce Zhang, and Christopher Ré. Caffe con troll: Shallow ideas to speed up deep learning. *CoRR*, abs/1504.04343, 2015.

[2] Dario Amodei, Rishita Anubhai, Eric Battenberg, Carl Case, Jared Casper, Bryan Catanzaro, Jingdong Chen, Mike Chrzanowski, Adam Coates, Greg Diamos, Erich Elsen, Jesse H. Engel, Linxi Fan, Christopher Fougner, Tony Han, Awni Y. Hannun, Billy Jun, Patrick LeGresley, Libby Lin, Sharan Narang, Andrew Y. Ng, Sherjil Ozair, Ryan Prenger, Jonathan Raiman, Sanjeev Satheesh, David Seetapun, Shubho Sengupta, Yi Wang, Zhiqian Wang, Chong Wang, Bo Xiao, Dani Yogatama, Jun Zhan, and Zhenyao Zhu. Deep speech 2: End-to-end speech recognition in english and mandarin. *CoRR*, abs/1512.02595, 2015.

[3] Nicolas Carion, Francisco Massa, Gabriel Synnaeve, Nicolas Usunier, Alexander Kirillov, and Sergey Zagoruyko. End-to-end object detection with transformers. *CoRR*, abs/2005.12872, 2020.

[4] William J. Dally, Yatish Turakhia, and Song Han. Domain-specific hardware accelerators. *Commun. ACM*, 63(7):48–57, jun 2020.

[5] Kaiming He, Xiangyu Zhang, Shaoqing Ren, and Jian Sun. Deep residual learning for image recognition. *CoRR*, abs/1512.03385, 2015.

[6] David Katz and Rick Gentile. *Embedded Media Processing*. Newnes (Elsevier), 2006.

[7] Hyoukjun Kwon, Michael Pellauer, and Tushar Krishna. MAESTRO: an open-source infrastructure for modeling dataflows within deep learning accelerators. *CoRR*, abs/1805.02566, 2018.

[8] Wim Meeus and Dirk Stroobandt. Data reuse buffer synthesis using the polyhedral model. *IEEE Transactions on Very Large Scale Integration (VLSI) Systems*, 26(7):1340–1353, 2018.

[9] Adam Paszke, Sam Gross, Francisco Massa, Adam Lerer, James Bradbury, Gregory Chanan, Trevor Killeen, Zeming Lin, Natalia Gimelshein, Luca Antiga, Alban Desmaison, Andreas Kopf, Edward Yang, Zachary DeVito, Martin Raison, Alykhan Tejani, Sasank Chilamkurthy, Benoit Steiner, Lu Fang, Junjie Bai, and Soumith Chintala. Pytorch: An imperative style, high-performance deep learning library. In H. Wallach, H. Larochelle, A. Beygelzimer, F. d'Alché-Buc, E. Fox, and R. Garnett, editors, *Advances in Neural Information Processing Systems 32*, pages 8024–8035. Curran Associates, Inc., 2019.

[10] Karen Simonyan and Andrew Zisserman. Very deep convolutional networks for large-scale image recognition, 2015.

[11] Ross Wightman. Pytorch image models. `https://github.com/rwightman/pytorch-image-models`, 2019.

[12] Yonghui Wu, Mike Schuster, Zhifeng Chen, Quoc V. Le, Mohammad Norouzi, Wolfgang Macherey, Maxim Krikun, Yuan Cao, Qin Gao, Klaus Macherey, Jeff Klingner, Apurva Shah, Melvin Johnson, Xiaobing Liu, Lukasz Kaiser, Stephan Gouws, Yoshikiyo Kato, Taku Kudo, Hideto Kazawa, Keith Stevens, George Kurian, Nishant Patil, Wei Wang, Cliff Young, Jason Smith, Jason Riesa, Alex Rudnick, Oriol Vinyals, Greg Corrado, Macduff Hughes, and Jeffrey Dean. Google's neural machine translation system: Bridging the gap between human and machine translation. *CoRR*, abs/1609.08144, 2016.

[13] Weijian Xu, Yifan Xu, Tyler Chang, and Zhuowen Tu. Co-scale conv-attentional image transformers.

[14] Xuan Yang, Mingyu Gao, Jing Pu, Ankita Nayak, Qiaoyi Liu, Steven Bell, Jeff Setter, Kaidi Cao, Heonjae Ha, Christos Kozyrakis, and Mark Horowitz. DNN dataflow choice is overrated. *CoRR*, abs/1809.04070, 2018.

[15] Xuan Yang, Mingyu Gao, Jing Pu, Ankita Nayak, Qiaoyi Liu, Steven Bell, Jeff Setter, Kaidi Cao, Heonjae Ha, Christos Kozyrakis, and Mark Horowitz. DNN dataflow choice is overrated. *CoRR*, abs/1809.04070, 2018.

[16] Chen Zhang, Guangyu Sun, Zhenman Fang, Peipei Zhou, Peichen Pan, and Jason Cong. Caffeine: Toward uniformed representation and acceleration for deep convolutional neural networks. *IEEE Transactions on Computer-Aided Design of Integrated Circuits and Systems*, 38(11):2072–2085, 2019.

[17] Xingkui Zhu, Shuchang Lyu, Xu Wang, and Qi Zhao. Tph-yolov5: Improved yolov5 based on transformer prediction head for object detection on drone-captured scenarios. *CoRR*, abs/2108.11539, 2021.